Magnetostructural Studies of Assembly Compounds Derived from Manganese(III)and Iron(III)Schiff Base Complexes and Hexacyanometalate(III)

宮坂, 等
九州大学理学研究科化学専攻

https://doi.org/10.11501/3134896

出版情報：九州大学, 1997, 博士（理学）, 課程博士
バージョン：
権利関係：

Chapter V

Two-dimensional Network Compounds Derived from the Reaction of $[Fe(salen)]^+$ and $[Fe(CN)_6]^{3-}$

V. 1 Introduction

In this Chapter it is attempted to construct bimetallic assembly compounds by the use of [Fe(salen)(Cl)] instead of Mn(III) Schiff base complexes. The $[Fe(salen)]^+$ is coordinatively unsaturated with respect to its labile axial sites like the $[Mn(salen)]^+$ and thence can be used as a counterpart building block for bimetallic extended compounds.[1] The $[Fe(salen)]^+$ has five unpaired electrons (S = 5/2) and the extended compounds derived from the $[Fe(salen)]^+$ produce spin-systems which differ from those derived from the $[Mn(salen)]^+$ and analogs (S = 2).

The reaction of [Fe(salen)(Cl)] with $[Fe(CN)_6]^{3-}$ (NEt_4^+ and K^+ salt) has produced two assembly compounds:

$[NEt_4][Fe(salen)]_2[Fe(CN)_6]\cdot H_2O$ (**V-1**)

$[Fe(salen)(MeOH)_2][Fe(salen)]_2[Fe(CN)_6]\cdot 3H_2O$ (**V-2**).

Both **V-1** and **V-2** exhibit a ferromagnetic phase transition which simultaneously cause a spontaneous magnetization, but they differ in magnetic behavior at lower temperature. The different magnetism of **V-1** and **V-2** is discussed by taking into consideration of the structure of **V-2**, showing a unique layered structure schematically shown in Scheme V.1.

Scheme V.1.

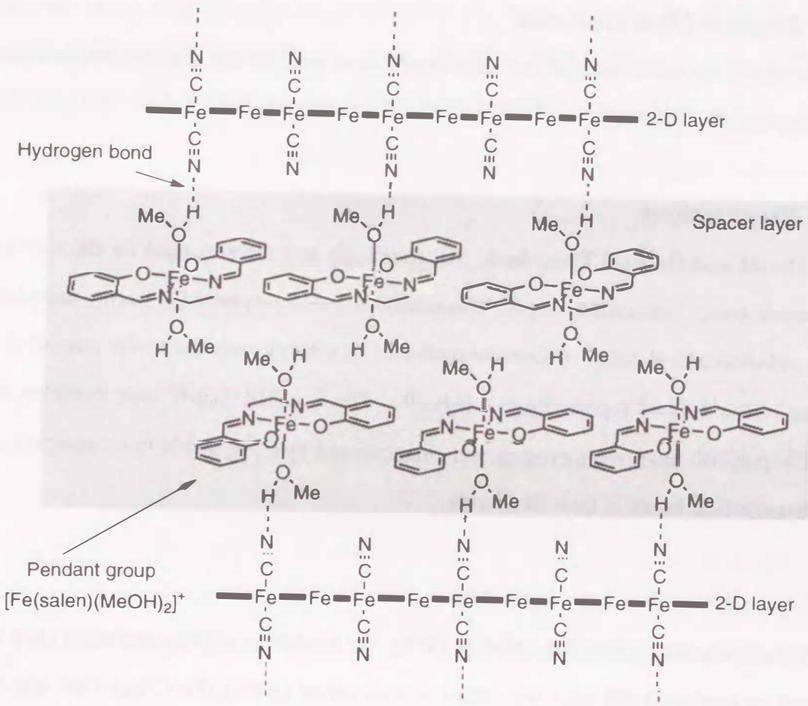

V. 2 Experimental

V. 2. 1 Physical Measurements

Essentially the same methods and apparatuses were used for the physical measurements in this Chapter (see Chapter I).

V. 2. 2 Preparations

Material and General Procedure. All chemicals and solvents used for the synthesis were reagent grade. Iron(III) Complex [Fe(salen)(Cl)] was prepared by mixing anhydrous iron(III) chloride and H_2salen in absolute methanol or ethanol with the molar ratio of 1 : 1 according to the method reported previously.[1b,i] The iron(III) Schiff base complex was obtained as purplish black miclocrystals and characterized by C, H, and N microanalyses and by the characteristic bands in their IR spectra.

Preparation of Bimetallic Assemblies.

$[NEt_4][Fe(salen)]_2[Fe(CN)_6]\cdot MeOH$ (V-1). To a solution of [Fe(salen)(Cl)] (179 mg, 0.5 mmol) in methanol (50 mL) was added a solution of $[NEt_4]_3[Fe(CN)_6]$ (301 mg, 0.5 mmol) in methanol (10 mL) and the purplish brown solution was stirred at room temperature to form purplish brown miclocrystals. They were collected by suction filtration, washed with a minimum amount of ethanol and dried *in vacuo*. The microanalyses and thermogravimetry analyses showed the presence of one methanol molecule as the crystal solvent. Anal. Calcd for $C_{47}H_{52}N_{11}O_5Fe_3$: C, 55.42; H, 5.15; N, 15.13; Fe, 16.45. Found; C, 55.35; H, 5.00; N, 15.47; Fe, 15.62. IR(KBr): ν[C=N (imine)] 1597 and 1638(broad) cm^{-1}; ν[C≡N (cyanide)] 2124 and 2141 cm^{-1}. M.p.: 218 °C.

$[Fe(salen)]_3[Fe(CN)_6]\cdot 2MeOH\cdot 3H_2O$ (V-2). To a solution of [Fe(salen)(Cl)] (179 mg, 0.5 mmol) in methanol (50 mL) was added slowly a solution of $K_3[Fe(CN)_6]$ (165 mg, 0.5 mmol) in water (20 mL) at room temperature. The resulting solution was kept to stand for 2 days and dark purplish-brown thin-plate crystals thus produced were collected by suction filtration, washed with a minimum amount of water and dried in air. The microanalyses and

thermogravimetric analyses showed the presence of two methanol molecules and three water molecules. Three water molecules were easily eliminated in air to give a dehydrated compound. Anal. Calcd for $C_{56}H_{50}N_{12}O_8Fe_4$: C, 54.14; H, 4.06; N, 13.53; Fe, 17.98. Found; C, 53.75; H, 3.67; N, 13.91; Fe, 14.64. IR(KBr): ν[C=N (imine)] 1599, 1618(broad) and 1636(broad) cm^{-1}; ν[C≡N (cyanide)] 2025(broad) and 2077 cm^{-1}. M.p.: 218 °C.

V. 2. 3 X-ray Data Collection and Reduction

Single crystals for **V-2** were prepared by the method described in the synthetic procedure. A single crystal for the crystallographic analysis was cut from a thin plate crystal in the mother liquid and sealed in a Lindemann glass capillary. Crystal dimensions are 0.35 × 0.07 × 0.40 mm. All measurements were made on a Rigaku AFC7R diffractometer with graphite monochromated Mo Kα radiation (λ = 0.71069 Å) and a 12 kW rotating anode generator. The data were collected at 20±1 °C using ω-2θ scan technique to a maximum 2θ value of 50.0 ° at a scan speed of 16.0 °/min (in omega). The weak reflections($I < 10.0\sigma(I)$) were rescanned (maximum of 4 scans) and the counts were accumulated to ensure good counting statistics. Stationary background counts were recorded on each side of the reflection. The ratio of peak counting time to background counting time was 2 : 1. Of the 5059 reflections which were collected, 4656 were unique. The diameter of the incident beam collimator was 1.0 mm, the crystal to detector distance was 235 mm, and the computer controlled detector aperture was set to 9.0 × 13.0 mm (horizontal vertical). The intensities of three representative reflections were measured after every 150 reflections. Over the course of the data collection, the standards reflections were monitored and the decay corrections were applied by a polynomial correction. An empirical absorption correction based on azimuthal scans of several reflections was applied. The data were corrected for Lorentz and polarization effects.

V. 2. 4 Solution and Refinement of Crystal Structures

The structure was solved by direct methods[2] and expanded using Fourier techniques.[3] The non-hydrogen atoms were refined anisotropically. Hydrogen atoms were refined isotropically. Full-matrix least-squares refinement based on 2482 observed reflections ($I > 3.00\sigma(I)$) were employed, where the unweighted and weighted agreement factors of $R = \Sigma||F_o|-|F_c||/\Sigma|F_o|$ and $Rw = [\Sigma w(|F_o|-|F_c|)^2/\Sigma w|F_o|^2]^{1/2}$ are used. The weighting scheme was based on counting statistics. Plots of $\Sigma w(|F_o|-|F_c|)^2$ versus $|F_o|$, reflection order in data collection, $\sin\theta/\lambda$ and various classes of indices showed no unusual trends. Neutral atomic scattering factors were taken from Cromer and Waber.[4] Anomalous dispersion effects were included in F_{calcd}; the values $\Delta f'$ and $\Delta f''$ were those of Creagh and McAuley.[5] The values for the mass attenuation coefficients are those of Creagh and Hubbel.[6] All calculations were performed using the teXsan crystallographic software package of Molecular Structure Corporation.[7] Crystal data and details of the structure determinations are summarized in Table V.1, and fractional positional parameters and equivalent isotropic thermal parameters for non-hydrogen atoms are listed in Table V.2. The fragility of the crystals made it difficult to improve the quality of the X-ray analysis.

Table V.1. Crystallographic Data for $[Fe(salen)(MeOH)_2][Fe(salen)]_2[Fe(CN)_6]\cdot 3H_2O\cdot MeOH$ (**V-2**)

	V-2		
Formula	$C_{56}H_{56}N_{12}O_{11}Fe_4$	α / deg	90
Formula Weight	1296.52	β / deg	96.74(2)
Crystal System	monoclinic	γ / deg	90
Space group	$P2_1/n$ (#14)	V / Å^3	6315(4)
T / degC	20	Z	4
λ / Å	0.71069	D_{cal} / gcm^{-3}	1.364
a / Å	13.495(7)	μ(MoKα) / cm^{-1}	9.64
b / Å	14.220(9)	No. of reflections	12271
c / Å	33.137(5)	R[a]	7.0
		Rw[b]	8.2

a; $R = \Sigma||F_o|-|F_c||/\Sigma|F_o|$, b; $Rw = [\Sigma w(|F_o|-|F_c|)^2/\Sigma w|F_o|^2]^{1/2}$, $w=1/[\sigma^2(Fo)]$.

Table V.2. Fractional Positional Parameters and Isotropic Equivalent Thermal Parameters for Non-Hydrogen Atoms for $[Fe(salen)(MeOH)_2][Fe(salen)]_2[Fe(CN)_6]\cdot 3H_2O\cdot MeOH$ (**V-2**)

atom	x	y	z	B(eq)
Fe(1)	0.3017(1)	0.8081(1)	-0.02802(5)	2.86(5)
Fe(2)	1/2	1/2	0	3.05(7)
Fe(3)	0.2008(1)	0.3057(1)	0.02324(5)	2.58(4)
Fe(4)	0	0	0	2.38(6)
Fe(5)	0.3652(2)	0.4826(2)	0.30189(6)	5.57(6)
O(1)	0.3919(6)	0.8888(5)	0.0029(2)	3.2(2)
O(2)	0.3215(6)	0.8253(6)	-0.0830(2)	3.8(2)
O(3)	0.2002(6)	0.3242(5)	0.0803(2)	3.1(2)
O(4)	0.0939(6)	0.3748(6)	-0.0044(2)	3.1(2)
O(5)	0.2434(8)	0.4422(8)	0.2699(3)	7.1(3)
O(6)	0.4711(8)	0.4192(8)	0.2818(3)	6.7(3)
O(7)	0.383(1)	0.5997(9)	0.2637(3)	8.6(4)
O(8)	0.3522(8)	0.3732(7)	0.3444(3)	6.0(3)
O(9)	0.987(1)	0.141(1)	0.2865(5)	17.7(8)
O(10)	1.128(2)	0.117(1)	0.3713(7)	28(1)
O(11)	0.822(2)	0.040(2)	0.333(1)	36(2)
N(1)	0.2454(8)	0.7711(8)	0.0254(3)	3.8(3)
N(2)	0.1914(8)	0.7072(7)	-0.0464(4)	3.6(3)
N(3)	0.3999(8)	0.6948(8)	-0.0206(4)	4.2(3)
N(4)	0.559(1)	0.575(1)	0.0882(5)	11.0(6)
N(5)	0.2980(8)	0.4207(7)	0.0207(3)	3.7(3)
N(6)	0.3290(7)	0.2213(7)	0.0375(3)	3.0(3)
N(7)	0.2421(8)	0.2664(7)	-0.0344(3)	3.5(3)
N(8)	0.1135(7)	0.1804(8)	0.0230(3)	3.2(3)
N(9)	0.1844(8)	-0.0872(7)	-0.0320(3)	3.2(3)
N(10)	-0.0641(9)	0.1014(8)	-0.0809(3)	4.4(3)
N(11)	0.272(1)	0.5664(8)	0.3362(3)	5.3(4)
N(12)	0.470(1)	0.5467(8)	0.3456(3)	4.5(3)
C(1)	0.416(1)	0.9006(9)	0.0427(4)	3.0(3)
C(2)	0.497(1)	0.9602(9)	0.0557(4)	3.2(3)
C(3)	0.525(1)	0.975(1)	0.0964(5)	4.7(4)
C(4)	0.476(1)	0.929(1)	0.1255(4)	6.0(5)
C(5)	0.398(1)	0.873(1)	0.1136(5)	5.7(5)
C(6)	0.366(1)	0.857(1)	0.0723(4)	3.8(4)
C(7)	0.280(1)	0.796(1)	0.0599(5)	4.7(4)
C(8)	0.154(1)	0.714(1)	0.0220(4)	4.4(4)
C(9)	0.156(1)	0.653(1)	-0.0138(5)	5.0(4)
C(10)	0.152(1)	0.696(1)	-0.0825(5)	4.5(4)
C(11)	0.181(1)	0.742(1)	-0.1178(5)	4.8(4)
C(12)	0.127(1)	0.728(1)	-0.1562(6)	7.0(5)
C(13)	0.147(1)	0.765(1)	-0.1923(5)	7.7(6)
C(14)	0.229(1)	0.820(1)	-0.1905(5)	6.7(5)
C(15)	0.289(1)	0.839(1)	-0.1536(5)	5.2(4)
C(16)	0.267(1)	0.802(1)	-0.1167(4)	3.6(4)
C(17)	0.436(1)	0.625(1)	-0.0134(4)	3.2(4)
C(18)	0.537(1)	0.547(1)	0.0567(5)	5.0(5)
C(19)	0.371(1)	0.4516(8)	0.0129(4)	3.0(3)
C(20)	0.277(1)	0.3267(8)	0.1088(4)	3.6(4)
C(21)	0.264(1)	0.363(1)	0.1471(4)	5.8(5)
C(22)	0.341(2)	0.370(1)	0.1780(5)	8.3(6)
C(23)	0.433(2)	0.340(1)	0.1731(5)	7.8(6)
C(24)	0.448(1)	0.299(1)	0.1360(5)	5.8(4)
C(25)	0.372(1)	0.288(1)	0.1044(4)	3.6(3)
C(26)	0.390(1)	0.2345(9)	0.0688(5)	3.6(4)
C(27)	0.354(1)	0.160(1)	0.0046(4)	4.5(4)
C(28)	0.338(1)	0.215(1)	-0.0342(4)	5.6(4)
C(29)	0.199(1)	0.291(1)	-0.0683(4)	5.1(4)
C(30)	0.113(1)	0.352(1)	-0.0744(4)	5.1(4)
C(31)	0.076(2)	0.373(1)	-0.1144(5)	9.7(7)
C(32)	-0.004(1)	0.434(1)	-0.1232(5)	8.7(6)
C(33)	-0.045(1)	0.477(1)	-0.0925(5)	5.2(4)
C(34)	-0.012(1)	0.459(1)	-0.0537(4)	3.6(4)
C(35)	0.066(1)	0.394(1)	-0.0428(4)	3.0(3)
C(36)	0.0706(8)	0.1113(8)	0.0167(4)	2.3(3)
C(37)	0.115(1)	-0.0509(8)	-0.0217(4)	2.6(3)
C(38)	-0.040(1)	0.064(1)	-0.0521(4)	3.2(3)
C(39)	0.154(1)	0.478(1)	0.2664(4)	5.9(5)
C(40)	0.092(1)	0.440(1)	0.2369(5)	7.7(6)
C(41)	-0.005(2)	0.473(1)	0.2303(5)	8.2(7)
C(42)	-0.040(1)	0.549(1)	0.2530(6)	7.9(6)
C(43)	0.029(1)	0.581(1)	0.2839(5)	7.0(5)
C(44)	0.124(1)	0.548(1)	0.2913(4)	5.2(4)
C(45)	0.179(1)	0.585(1)	0.3259(5)	5.9(5)
C(46)	0.330(1)	0.601(1)	0.3752(4)	6.8(5)
C(47)	0.436(1)	0.624(1)	0.3689(5)	5.7(5)
C(48)	0.556(1)	0.519(1)	0.3550(4)	5.0(4)
C(49)	0.604(1)	0.442(1)	0.3360(4)	5.0(4)
C(50)	0.700(1)	0.411(1)	0.3509(5)	6.0(5)
C(51)	0.751(1)	0.335(2)	0.3335(6)	7.6(6)
C(52)	0.709(1)	0.293(2)	0.3004(6)	8.6(7)
C(53)	0.616(2)	0.317(1)	0.2844(5)	7.8(6)
C(54)	0.562(1)	0.396(1)	0.3004(5)	5.9(5)
C(55)	0.297(3)	0.689(3)	0.250(1)	27(2)
C(56)	0.343(2)	0.275(2)	0.3333(7)	17(1)

V. 3 Results and Discussion

V. 3. 1 General Characterization

The syntheses of **V-1** and **V-2** are schematically shown in Scheme V.2. When $[NEt_4]_3[Fe(CN)_6]$ was used and the reaction was carried out in methanol, **V-1** was produced immediately. For the synthesis of **V-2**, $K_3[Fe(CN)_6]$ was used instead of $[NEt_4]_3[Fe(CN)_6]$ and the reaction was carried out in a methanol / water mixed solvent. It should be noteworthy that the reaction between [Fe(salen)(Cl)] and $A_3[Fe(CN)_6]$, regardless of the 1 : 1 molar ratio of the components, gave the different aggregates, 2 : 1 (**V-1**) or 3 : 1 (**V-2**), as a function of the cation A^+. Some solvent molecules are contained as the crystallization solvent or donor ligand in **V-1** and **V-2**. In **V-1** one methanol is involved as a crystal solvent that is easily eliminated. The thermogravimetric analyses indicated the release of the methanol and water solvents to start at about 30 °C. In **V-2**, two methanol molecules and three water molecules are contained; the water molecules are involved in the crystal lattice and two methanol molecules are coordinated to $[Fe(salen)]^+$ species as revealed by X-ray crystallography later. The thermogravimetric analyses have indicated that the water molecules dehydrated at 37 - 93 °C but two methanol molecules are not eliminated below 100 °C. This fact and the comparison between **V-1** and **V-2** suggest that two methanol molecules coordinate to $[Fe(salen)]^+$ forming $[Fe(salen)(MeOH)_2]^+$ and this solvated species exists as a cation in the ordered network of **V-2**. It is presumed that **V-1** and **V-2** have an essentially similar network except for the cation (NEt_4^+ for **V-1** and $[Fe(salen)(MeOH)_2]^+$ for **V-2**).

Scheme V.2

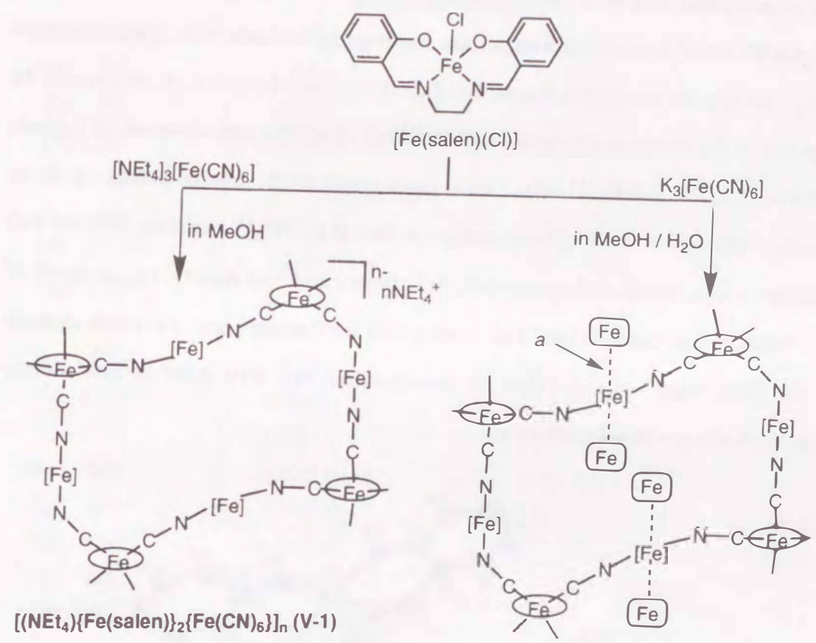

V. 3. 2 Structural Studies

Structural Description of [Fe(salen)]$_3$[Fe(CN)$_6$]·2MeOH·3H$_2$O (V-2). An ORTEP view of the pentanuclear unit with the numbering scheme of the unique atoms is shown in Figure V.1, and the bond distances and angles are summarized in Table V.3. Two iron atoms of $[Fe(CN)_6]^{3-}$ occupy the inversion centers, Fe2 (1/2, 1/2, 0) and Fe4 (0, 0, 0), as a result, the atom occupancy of these iron atoms was situated as half of weight and all atoms of formula unit [Fe(salen)]$_3$[Fe(CN)$_6$]·2MeOH·3H$_2$O were determined as the unique atoms by X-ray crystallographic calculation. Four cyanide groups of each $[Fe(CN)_6]^{3-}$ moieties, Fe2 and Fe4 moieties, bridge to two Fe(III) salen moieties, Fe1 moiety and Fe3 moiety, by *cis*-mode of $[Fe(CN)_6]^{3-}$ moieties (as same as both Fe2 moiety and Fe4 moiety) and other two cyanide groups of the $[Fe(CN)_6]^{3-}$ do not relate to coordination, but N10 atom of Fe4 moiety participate to the hydrogen bond (*vide infra*).

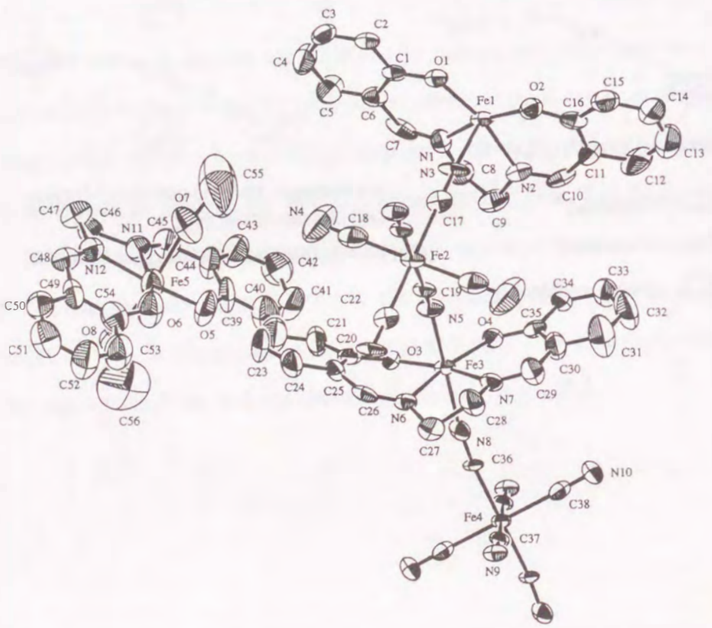

Figure V.1. ORTEP drawing of a pentanuclear structure [{Fe(salen)}$_3${Fe(CN)$_6$}(MeOH)$_2$] (**V-2**) with the atom numbering scheme of the unique atoms, showing 50 % probability ellipsoids and three water molecules as the crystal solvents are omitted for clearly, where Fe2 and Fe4 atoms have an occupancy of half weight because of the inversion center.

Table V.3. Relevant Bond Distances (Å) and Angles (deg) for **V-2** with the Estimated Standard Deviations in Parentheses

	Bond Distances (Å)		
Fe1 - O1	1.886(8)	Fe3 - N8	2.14(1)
Fe1 - O2	1.890(8)	N8 - C36	1.15(1)
Fe1 - N1	2.07(1)	Fe4 - C36	1.90(1)
Fe1 - N2	2.11(1)	Fe4 - C37	1.93(1)
Fe1 - N3	2.08(1)	Fe4 - C38	1.97(1)
Fe1 - N9*	2.17(1)	N9 - C37	1.15(1)
N3 - C17	1.12(1)	N10 - C38	1.11(1)
Fe2 - C17	2.01(1)	Fe5 - O5	1.94(1)
Fe2 - C18	2.00(2)	Fe5 - O6	1.877(10)
Fe2 - C19	1.97(1)	Fe5 - O7	2.12(1)
N4 - C18	1.12(2)	Fe5 - O8	2.12(1)
N5 - C19	1.14(1)	Fe5 - N11	2.15(1)
Fe3 - N5	2.10(1)	Fe5 - N12	2.11(1)
Fe3 - O3	1.910(8)	O7 - C55	1.74(4)
Fe3 - O4	1.892(8)	O8 - C56	1.44(3)
Fe3 - N6	2.112(10)		
Fe3 - N7	2.13(1)		
	Hydrogen Bond Distances (Å)		
O8···N10*	2.62(1)		
	Bond Angles (deg)		
Fe1 - N3 - C17	165(1)	Fe4 - C36 - N8	173(1)
Fe2 - C17 - N3	179(1)	Fe4 - C37 - N9	173(1)
Fe2 - C19 - N5	177(1)	Fe1 - N9* - C37*	154(1)
Fe3 - N5 - C19	150(1)	Fe5 - O7 - C55	127(1)
Fe3 - N8 - C36	168(1)	Fe5 - O8 - C56	123(1)

Four iron moieties of Fe1, Fe2, Fe3, and Fe4 form the two-dimensional network structure consisting of a cyclic octanuclear net unit [-Fe1-NC-Fe2-CN-Fe3-NC-Fe4-CN-]$_2$ as shown in Figure V.2a, where two-dimensional network structure is a view projected along the *c*-axis. One the other hand, Fe5 salen moiety is mononuclear cation, where iron atom has an octahedral coordination geometry consisting of the coordination of N_2O_2 quadridentate chelate ligand ($salen^{2-}$) and two monodentate methanol molecules, and situates between

layers by the hydrogen bond between hydroxo group O8-H of methanol and N10 of cyanide group with the distance of O8···N10 = 2.62(1) Å. The Figure V.2b and V.2c show the stacking of two adjacent layers, where that is a view projected perpendicular to the *c*-axis (in Figure V.2c, carbon atoms and water molecules as a crystal solvent are omitted for clarity). As shown in Figure V.2b and V.2c, Fe5 salen moiety positions on the interlayer like a "pendant" with hydrogen bond or "sandwich type" and this "pendant" is attached to both side of layer (upside and downside) against the inversion center Fe4 (O8···N10-C38-Fe4-C38'-N10'···O8') and this "pendant mode" appears one every other $[Fe(CN)_6]^{3-}$ moiety of octanuclear net unit $[-Fe1\text{-}NC\text{-}Fe2\text{-}CN\text{-}Fe3\text{-}NC\text{-}Fe4\text{-}CN\text{-}]_2$. All three Fe(III) salen moieties have an octahedral coordination geometry in which the equatorial sites are occupied by the N_2O_2 quadridentate salen Schiff base ligand, however, as shown in Figure V.3, Fe3 salen moiety has a large strain between the least square basal planes consisting of benzene moiety (Fe3 salen: 30.34°), because of the steric hindrance between Fe3 salen moiety and "pendant" Fe5 salen moiety, while in Fe1 and Fe5 salen moieties, the strain are hardly shown (Fe1 salen: 8.91° and Fe5 salen: 7.37°). The two-dimensional network structure of this complex is similar to that of $K[Mn(3\text{-}MeOsalen)]_2[Fe(CN)_6]\cdot 2DMF$ (**I-3b**), $[NEt_4][Mn(salen)]_2[Fe(CN)_6]$ (**I-4**), or $[NEt_4][Mn(5\text{-}Clsalen)]_2[Fe(CN)_6]$ (**III-4**) described above Chapter, where these complexes have a two-dimensional network structure consisting of a cyclic octanuclear net unit $[-Mn\text{-}NC\text{-}Fe\text{-}CN\text{-}]_4$. But the distance of the interlayer is very different [this compound: 16.57 Å, $K[Mn(3\text{-}MeOsalen)]_2[Fe(CN)_6]\cdot 2DMF$ (**I-3b**): 13.75 Å, $[NEt_4][Mn(salen)]_2[Fe(CN)_6]$ (**I-4**): 13.00 Å, $[NEt_4][Mn(5\text{-}Clsalen)]_2[Fe(CN)_6]$ (**III-4**): 13.10 Å]. We can expect that the reason of this compound has a largest interlayer distance is due to the steric factor of Fe5 salen molecules against each layers.

(a)

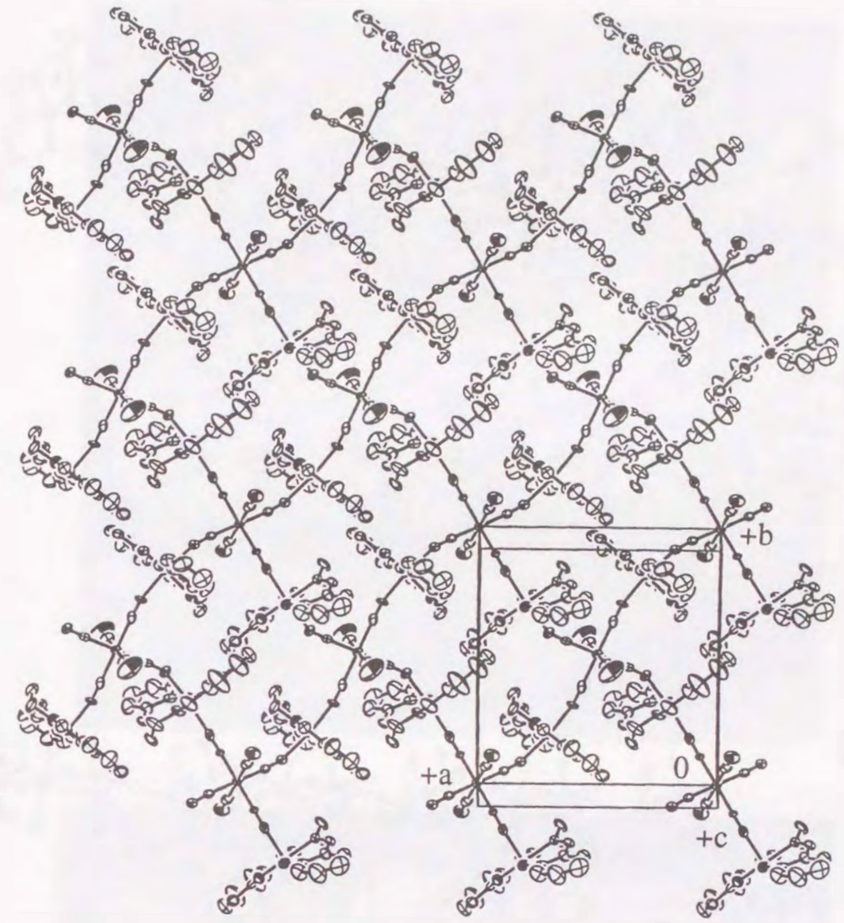

Figure V.2. (a) Two-dimensional network structure of **V-2** consisting of a cyclic octanuclear net unit $[-Fe1\text{-}NC\text{-}Fe2\text{-}CN\text{-}Fe3\text{-}NC\text{-}Fe4\text{-}CN\text{-}]_2$. (b) Stacking of the adjacent two-dimensional layers along the *c*-axis, where the mononuclear species $[Fe(salen)(MeOH)_2]^+$ is positioned between layers. (c) Formation of the hydrogen bond between two-dimensional layer and $[Fe(salen)(MeOH)_2]^+$, where the hydrogen bonds appear to both side of layer (upside and downside) against the inversion center Fe4 (O8···N10-C38-Fe4-C38'-N10'···O8') and one every other $[Fe(CN)_6]^{3-}$ moiety of octanuclear net unit $[-Fe1\text{-}NC\text{-}Fe2\text{-}CN\text{-}Fe3\text{-}NC\text{-}Fe4\text{-}CN\text{-}]_2$.

(b)

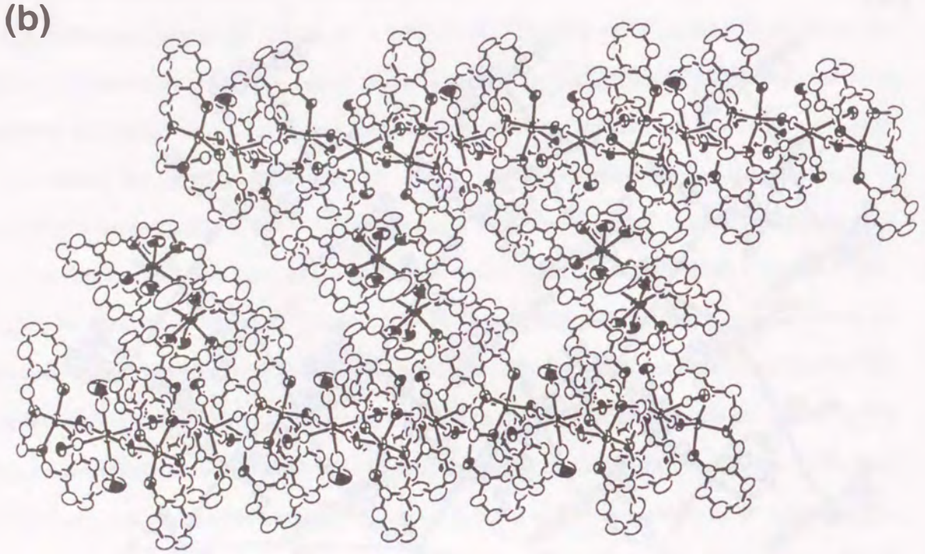

(c)

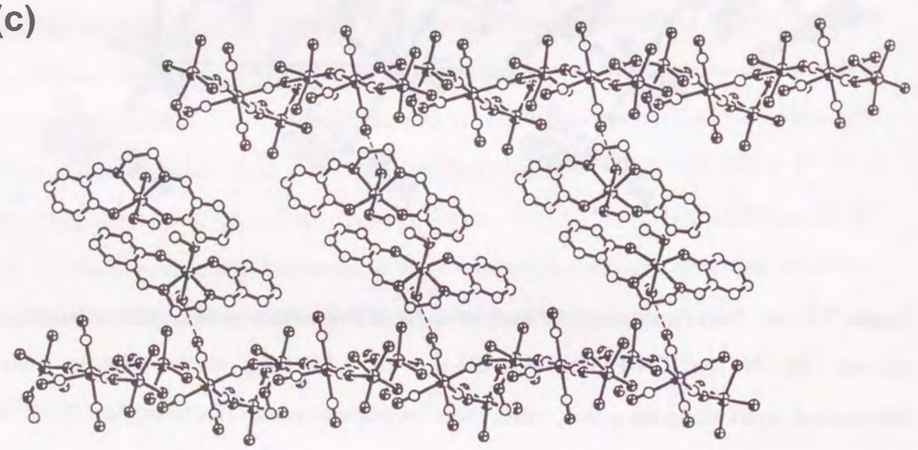

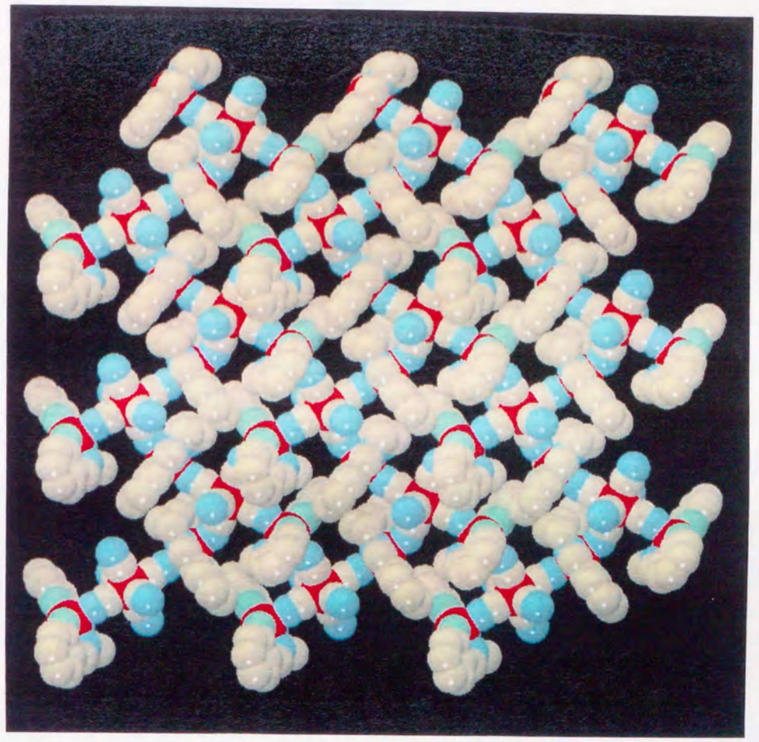

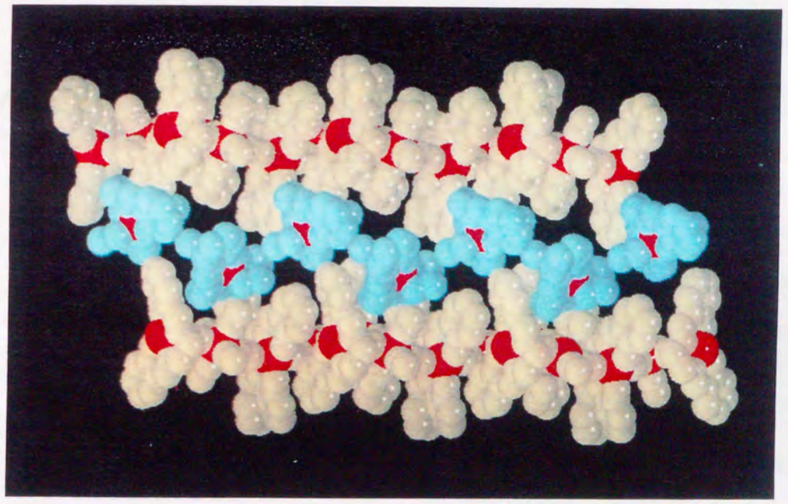

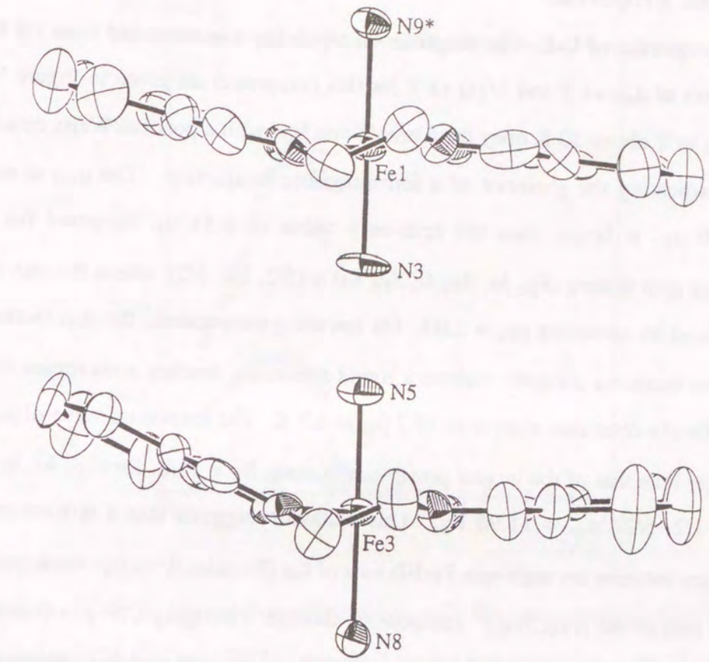

Figure V.3. Stereochemistry of Fe(III) salen components constituting compound **V-2**, where all views are projected perpendicular to the axial direction of iron octahedral coordination geometry.

V. 3. 3 Magnetic Properties

Magnetic properties of V-1. The magnetic susceptibility was measured from 1.9 K to 300 K and the plots of μ_{eff} *vs* T and $1/\chi_M$ *vs* T for this compound are given in Figure V.4. The plots of $1/\chi_M$ *vs* T above 30 K obey the Curie-Waiss law with a positive Weiss constant of θ = +7.2 K, indicating the presence of a ferromagnetic interaction. The μ_{eff} at room temperature, 8.90 μ_B, is larger than the spin-only value of 8.54 μ_B expected for the magnetically dilute spin system (S_{Fe} *hs*, S_{Fe} *ls*, S_{Fe} *hs*) = (5/2, 1/2, 5/2), where the spin only value was calculated by assuming g_{Fe} = 2.00. On lowering temperature, the μ_{eff} increases gradually and then increases abruptly without a round minimum, reaches a maximum of 35 μ_B at 7.4 K and finally decreases sharply to 19.7 μ_B at 1.9 K. The maximum value of μ_{eff} is significantly larger than that of the largest possible spin state, S_T = 11/2, for (S_{Fe} *hs*, S_{Fe} *ls*, S_{Fe} *hs*) = (5/2, 1/2, 5/2), μ_{so} = 11.96 μ_B. This behavior suggests that a ferromagnetic interaction operates between the high-spin Fe(III) ions of the $[Fe(salen)]^+$ components and the low-spin Fe(III) ions of the $[Fe(CN)_6]^{3-}$ components through a bridging CN^- group and the ferromagnetic ordering is built to high dimension. The sharp increase and then decrease are

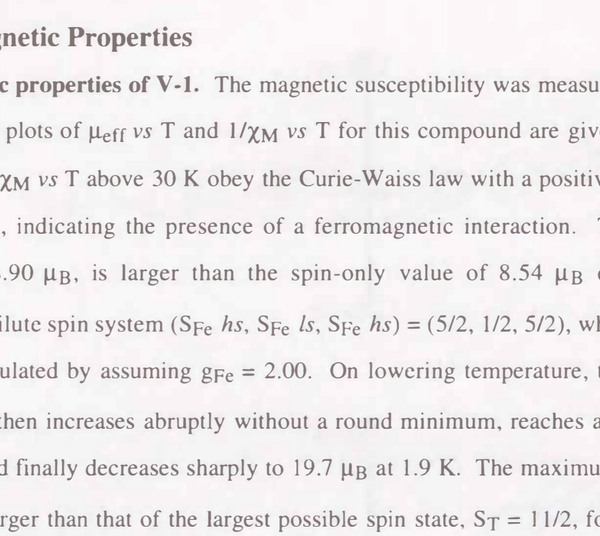

Figure V.4. Plots of the effective magnetic moment μ_{eff} and $1/\chi_M$ per $[Fe_2Fe]$ unit *vs* T for **V-1**.

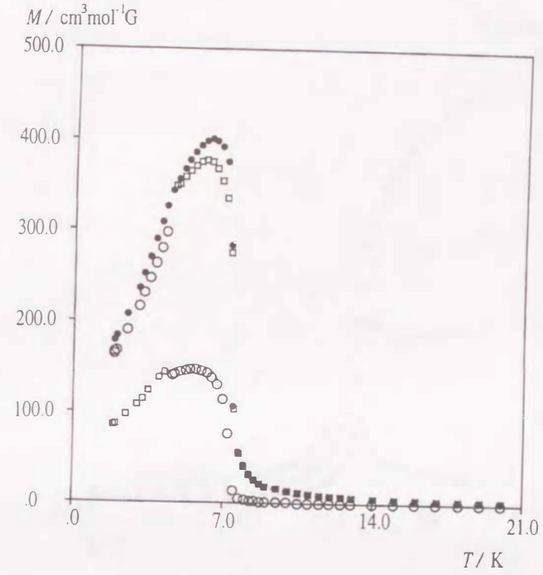

Figure V.5. FCM (field-cooled magnetization *vs* T; ●) curve under 3 Oe, RM (remnant magnetization *vs* T; ○), and ZFCM (zero-field cooled magnetization *vs* T; □) for **V-1**.

confirmed by the field-cooled magnetization curve taken under 3 Oe from 20 to 1.9 K (Figure V.5). At first, the magnetization shows a rapid increase below ca. 9 K and a break in the curve around T_c = 7.5 K, and then it reached a maximum at 6 K and decreased gradually below 6K to 1.9 K. The decrease at low temperature suggests the second ordering of the ferromagnetic ordered spin and it must be the antiferromagnetic ordering between interlayers, this behavior is typical of metamagnet. When the field was switched off at 1.9 K, a remnant magnetization was observed. RM has a transition at 4 K in which the magnetization abruptly decreases and then completely vanishes at T_c upon warming. Finally, the zero-field cooled magnetization, obtained by cooling in zero field and warming under 3 Oe, was measured. ZFCM curve also has a break at 4 K and then reaches maximum peak as same as FCM curve (Figure V.5). The transition at 4 K on RM and ZFCM exhibits the substantial metamagnetc transition.

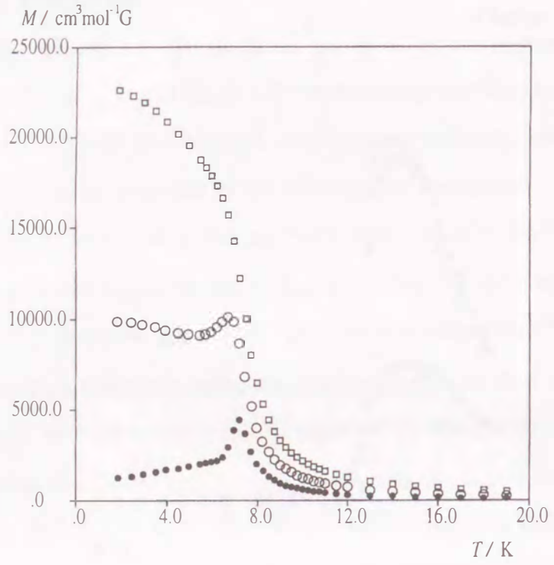

Figure V.6. FCM (field-cooled magnetization *vs* T) curve under 100 Oe (●), 300 Oe (○), and 500 Oe (□) for **V-1**.

In order to investigate the magnetic behavior below at 7.5 K, which is the temperature of ferromagnetic phase transition, the field-cooled magnetizations were measured under some external magnetic fields, 100, 300, and 500 Oe, and are given in Figure V.6. The decrease in the magnetization curve at 7.5 K is observed when the applied magnetic field is 300 Oe or lower and moreover, it at 100 Oe decreases more sharply than that at 300 Oe. This fact suggests that this compound has a metamagnetic character, which implies that an external magnetic field of 500 Oe is strong enough to overcome the antiferromagnetic interaction operating between interlayers but the applied field of 300 Oe is insufficient to overcome it. To confirm the metamagnetic transition, and to better characterize the antiferromagnetic to ferromagnetic transition, the magnetization was measured as a function of the external magnetic field at various temperatures. The results are given in Figure V.7. The magnetization curve at 1.9 K shows a sudden spin flopping at 370 Oe to increase abruptly. The spin flopping at 6 K occurs more slowly and no such spin flopping in magnetization occurs at 8 K, because the measured temperature is lower than the transition temperature.

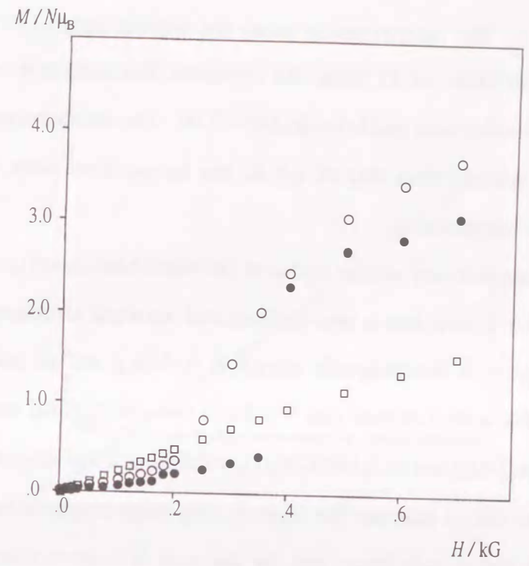

Figure V.7. Magnetization as a function of the applied magnetic field up to 1 kOe for **V-1** at 1.9 K (●), 6 K (○), and 8 K (□).

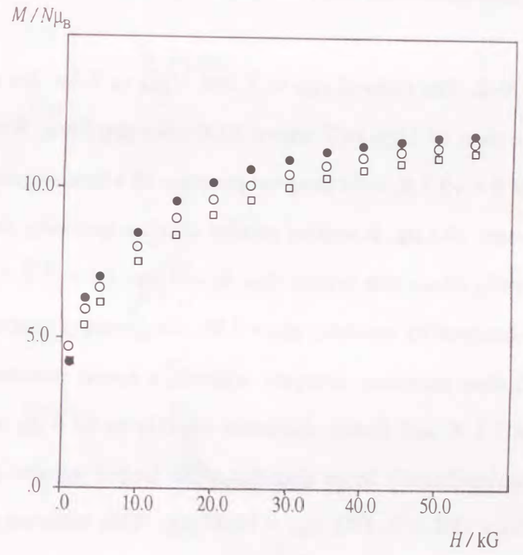

Figure V.8. Magnetization as a function of the applied magnetic field up to 55 kOe for **V-1** at 1.9 K (●), 4 K (○), and 6 K (□).

Magnetizations as the function of the applied magnetic field up to 55 kOe were measured and are shown in Figure V.8. The magnetization under the applied field of 55 kOe at 1.9 K reaches to the saturation value of 11 $N\mu_B$, the complete ferromagnetic coupling value $N\mu_B(2g_{Fe}S_{Fe}(hs) + g_{Fe}S_{Fe}(ls))$ with $g_{Fe}(hs) = g_{Fe}(ls) = 2.00$. The saturation of magnetization at 4 and 6 K is more difficult than that of 1.9 K, the temperature more lower than T_c (ferromagnetic transition temperature).

This magnetic behavior is very similar to that of $[K\{Mn(3\text{-}MeOsalen)\}_2\{Fe(CN)_6\}]_n$ (**I-3**), described in Chapter I, that has a two-dimensional network structure and shows a metamagnetic nature due to a ferromagnetic intralayer ordering and an antiferromagnetic interlayer interaction. The author expects that **V-1** has a two-dimensional network structure similar to that of $[K\{Mn(3\text{-}MeOsalen)\}_2\{Fe(CN)_6\}]_n$ exhibiting a metamagnetic nature; the abrupt increase in magnetization indicates the onset of long-range magnetic ordering due to a ferromagnetic coupling within each layers and the decrease in magnetization below 7.7 K indicates the presence of interlayer antiferromagnetic interaction. The cation $(NEt_4)^+$ of **V-1** must situate on interlayer like the 2-D compound $[(NEt_4)\{Mn(5\text{-}Clsalen)\}_2\{Fe(CN)_6\}]_n$ (**III-4**) in which the interlayer magnetic interaction is antiferromagnetic.

Magnetic properties of V-2. The plots of μ_{eff} *vs* T and $1/\chi_M$ *vs* T for this compound are given in Figure V.9. The plots of $1/\chi_M$ *vs* T above 30 K obey the Curie-Waiss law with a positive Weiss constant of $\theta = +5.7$ K, indicating the presence of a ferromagnetic interaction. The μ_{eff} at room temperature, 10.1 μ_B, is slightly smaller than the spin-only value of 10.4 μ_B expected for the magnetically dilute spin system (S_{Fe} *hs* × 3, S_{Fe} *ls*) = (5/2 × 3, 1/2), where the spin only value was calculated by assuming $g_{Fe} = 2.00$. On lowering temperature, the μ_{eff} increases gradually and then increases abruptly without a round minimum, reaches a maximum of 72.6 μ_B at 7.1 K and finally decreases slightly to 62.6 μ_B at 4.2 K. The maximum value of μ_{eff} is significantly larger than that of the largest possible spin state, S_T = 8, for (S_{Fe} *hs* × 3, S_{Fe} *ls*) = (5/2 × 3, 1/2), μ_{so} = 16.97 μ_B. This behavior suggests that a ferromagnetic interaction operates between the high-spin Fe(III) ions of the $[Fe(salen)]^+$ components and the low-spin Fe(III) ions of the $[Fe(CN)_6]^{3-}$ components through a bridging CN^- group, and the ferromagnetic ordering is built to a high dimension as same as the

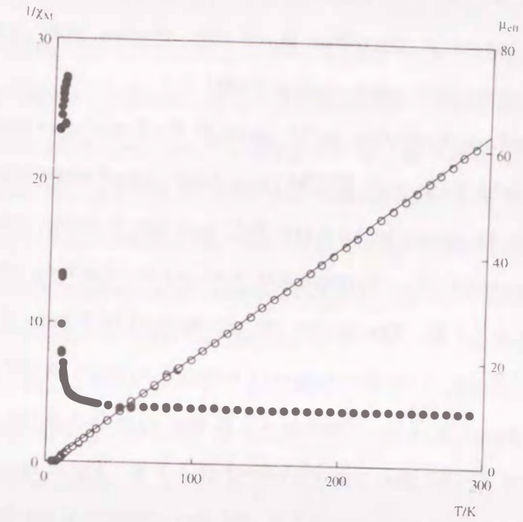

Figure V.9. Plots of the effective magnetic moment μ_{eff} and $1/\chi_M$ per $[Fe_3Fe]$ unit *vs* T for **V-2**.

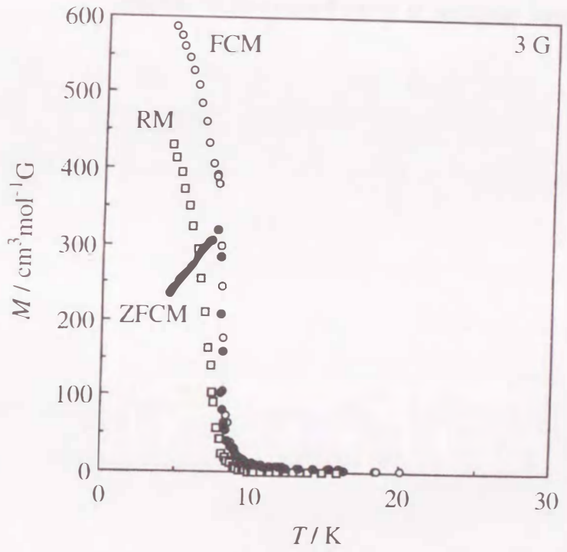

Figure V.10. FCM (field-cooled magnetization *vs* T; ○) curve under 3 Oe, RM (remnant magnetization *vs* T; □), and ZFCM (zero-field cooled magnetization *vs* T; ●) for **V-2**.

magnetic behavior of compound **V-1**. However, the author expects that this compound is two-dimensional compound like **V-1**. Because one of $[Fe(salen)]^+$ components is isolated as $[Fe(salen)(MeOH)_2]^+$, magnetic contribution of this species does not relate to the ferromagnetic ordering in the bulk (see structural study).

FCM (field-cooled magnetization *vs* T) curve of **V-2** was obtained by cooling the sample under a weak field, 3 Oe, and ZFCM (zero-field-cooled magnetization *vs* T) curve was obtained by cooling the sample under a zero field and then warming under a weak field, 3 Oe. RM (remnant magnetization *vs* T) curve was obtained by switching off the applied field after measuring FCM at 4.2 K. The results are represented in Figure V.10. FCM curve increased sharply at 7.7 K due to the ferromagnetic ordering to reach to 590 $cm^3mol^{-1}G$ at 4.2 K. Remnant magnetization was measured at 4.2 K that vanished at the T_c = 7.7 K upon warming. The peak of ZFCM also was measured at 7.7 K. These results show that the ferromagnetic phase transition occurs at 7.7 K and this compound exhibits a spontaneous magnetization typical of a ferromagnet.

This compound **V-2** has an efflorescence nature due to the release of the water molecules for crystallization. It should be mentioned that the desolvated sample of **V-2** does not show the ferromagnetic transition as found for crystalline samples.

V. 4 Conclusion

Two Fe(III) extended compounds, $[(NEt_4)\{Fe(salen)\}_2\{Fe(CN)_6\}]_n \cdot MeOH$ (**V-1**) and $[\{Fe(salen)\}_3\{Fe(CN)_6\}(MeOH)_2]_n \cdot 3nH_2O$ (**V-2**), have been synthesized separately. They have the same two-dimensional layer structure consisting of cyclic octanuclear net unit $[-Fe_1-NC-Fe_2-CN-]_4$ [Fe_1 = high spin iron(III), Fe_2 = low spin iron(III)]. The intralayer magnetic interaction between the high-spin iron(III) and low-spin iron(III) is ferromagnetic in both compounds leading to a spontaneous magnetization, but the two compounds showed different interlayer magnetic interactions. In compound **V-1**, tetraethylammonium cation locates in the interlayer, as well as $[(NEt_4)\{Mn(5\text{-}Clsalen)\}_2\{Fe(CN)_6\}]_n$, and the antiferromagnetic interaction operates between the layers. Compound **V-1** is a typical metamagnet. In **V-2**, the cation $[Fe(salen)(MeOH)_2]^+$ situates between the layers, and operates a ferromagnetic interaction between the layers.

Compound **V-2** illustrates one type of hybrid two-dimensional layered compounds. Such hybrid two-dimensional layered compounds, constructed by alternating different layers, are of great interest in view of the development of new functional materials.

V. 5 References

1. (a) Nishida, Y.; Oshio, S.; Kida, S. *Chem. Lett.* **1975**, 59. (b) Nishida, Y.; Oshio, S.; Kida, S. *Bull. Chem. Soc. Jpn.* **1977**, 50, 119. (c) Nishida, Y.; Oshio, S.; Kida, S. *Inorg. Chim. Acta* **1977**, 23, 59. (d) Nishida, Y.; Oshio, S.; Kida, S.; Maeda, Y. *Inorg. Chim. Acta* **1978**, 26, 207. (e) Nishida, Y.; Sumita, A.; Hayashida, H.; Oshima, H.; Kida, S.; Maeda, Y. *J. Coord. Chem.* **1979**, 9, 161. (f) Gerloch, M.; Lewis, J.; Mabbs, F. E.; Richards, A. *J. Chem. Soc. (A)* **1968**, 112. (g) Matsumoto, N.; Kimoto, K.; Nishida, Y.; Ohyoshi, A.; Maeda, Y. *Chem. Lett.* **1984**, 479. (h) Matsumoto, N.; Ohta, S.; Yoshimura, C.; Ohyoshi, A.; Kohata, S.; Okawa, H.; Maeda, Y. *J. Chem. Soc. Dalton Trans.* **1985**, 2575. (i) Maeda, Y.; Takashima, Y.; Matsumoto, N.; Ohyoshi, A. *J. Chem. Soc. Dalton Trans.* **1986**, 1115. (j) Nishida, Y.; Kino, K.; Kida, S. *J. Chem. Soc. Dalton Trans.* **1987**, 1157. (k) Fukuya, M.; Ohba, M.; Motoda, K.; Matsumoto, N.; Okawa, H.; Maeda, Y. *J. Chem. Soc. Dalton Trans.* **1993**, 3277.
2. SHELXS86: Sheldrick, G. M. In *Crystallographic Computing 3*, Sheldrick, G. M.; Kruger, C.; Goddard, R. Eds., Oxford University Press, **1985**, pp 175-189.
3. DIRDIF92: Beurskens, P. T.; Admiraal, G.; Beurskens, G.; Bosman, W. P.; Garcia-Granda, S.; Gould, R. O.; Smits, J. M. M.; Smykalla, C. The DIRDIF program system. Technical Report of the Crystallography Laboratory; University of Nijmegen: The Netherlands, 1992.
4. Cromer, D. T.; Waber, J. T. *International Tables for Crystallography*; The Kynoch Press: Birmingham, England, 1974; Vol. IV, Table 2.2A.
5. Creagh, D. C.; McAuley, W. J. In *In International Tables for Crystallography*; Wilson, A. J. C., Ed., Kluwer Academic Publishers: Boston, 1992; Vol. C, pp 219-222, Table 4.2.6.8.
6. Creagh, D. C.; Hubbel, J. H. In *International Tables for Crystallography*; Wilson, A. J. C., Ed., Kluwer Academic Publishers: Boston, 1992; Vol. C, pp 200-206, Table 4.2.4.3.
7. teXsan: Crystal Structure Analysis Package, Molecular Structure Corporation, 1985, 1992.

General Conclusion

The reaction between manganese(III) or iron(III) complexes of salen-type (acacen-type) Schiff bases and hexacyanoferrate(III) afforded various types of multi-dimensional structural compounds (thirty three compounds descrived in Chapter I - V) given as follows. In Figure 1 are summarized the assembly compounds obtained in this study. Their synthetic methods and structures are summarized in Scheme 1.

$[NEt_4]_2[Mn(acacen)][Fe(CN)_6]$ (**I-1**)

rac-$[NEt_4]_2[Mn(acacmen)][Fe(CN)_6]$ (**I-2**)

$K[Mn(3\text{-}MeOsalen)]_2[Fe(CN)_6]$ (**I-3a**)

$K[Mn(3\text{-}MeOsalen)]_2[Fe(CN)_6]\cdot 2DMF$ (**I-3b**)

$[NEt4][Mn(salen)]_2[Fe(CN)_6]$ (**I-4**)

$[Mn(saltmen)]_4[Fe(CN)_6]ClO_4\cdot 3H_2O$ (**I-5a**)

$[Mn(saltmen)]_4[Fe(CN)_6]ClO_4\cdot H_2O$ (**I-5b**)

$[Mn(saltmen)]_4[Co(CN)_6]ClO_4\cdot 2H_2O$ (**I-6**)

$K[Mn(3\text{-}MeOsalen)]_2[Co(CN)_6]\cdot 2DMF$ (**II-1a**)

$K[Mn(3\text{-}MeOsalen)]_2[Co(CN)_6]\cdot 4H_2O$ (**II-1b**)

$K[Mn(3\text{-}MeOsalen)]_2[Mn(CN)_6]\cdot H_2O$ (**II-2**)

$K[Mn(3\text{-}MeOsalen)]_2[Cr(CN)_6]\cdot H_2O$ (**II-3**)

$K[Mn(5\text{-}Clsalen)(H_2O)]_2[Fe(CN)_6]\cdot 2H_2O$ (**III-1**)

$K[Mn(5\text{-}Brsalen)(H_2O)]_2[Fe(CN)_6]\cdot 2H_2O$ (**III-2**)

$[NEt_4][Mn(5\text{-}Clsalen)(H_2O)]_2[Fe(CN)_6]\cdot H_2O$ (**III-3a**)

$[NEt_4][Mn(5\text{-}Clsalen)]_2[Fe(CN)_6]$ (desolvated compound) (**III-3b**)

$[NEt_4][Mn(5\text{-}Clsalen)]_2[Fe(CN)_6]$ (**III-4**)

$[NEt_4]_2[Mn(saldmen)(H_2O)][Fe(CN)_6]\cdot 2H_2O$ (**IV-1a**)

$[NEt_4]_2[Mn(saldmen)][Fe(CN)_6]$ (desolvated compound) (**IV-1b**)

rac-$[NEt_4][Mn(salmen)(MeOH)]_2[Fe(CN)_6]$ (**IV-2a**)

rac-$[NEt_4][Mn(salmen)]_2[Fe(CN)_6]$ (desolvated compound) (**IV-2b**)

rac-[NEt_4][Mn(salcy)(MeOH)]$_2$[Fe(CN)$_6$] (**IV-3a**)

rac-[NEt_4][Mn(salcy)]$_2$[Fe(CN)$_6$] (desolvated compound) (**IV-3b**)

(*R*, *R*)-[NEt_4][Mn(salcy)(H_2O)]$_2$[Fe(CN)$_6$]·MeOH (**IV-4a**)

(*R*, *R*)-[NEt_4][Mn(salcy)]$_2$[Fe(CN)$_6$] (desolvated compound) (**IV-4b**)

[Mn(saltmen)(H_2O)]$_4$[Fe(CN)$_6$]ClO_4 (**IV-5a**)

[Mn(saltmen)]$_4$[Fe(CN)$_6$]ClO_4 (desolvated compound) (**IV-5b**)

[Mn(salen)]$_3$[Fe(CN)$_6$]·0.5H_2O (**IV-6a**)

[{Mn(salen)}$_3${Fe(CN)$_6$}(H_2O)$_2$(MeOH)$_2$]·3H_2O·MeOH (**IV-6b**)

rac-[Mn(salcy)]$_4$[Fe(CN)$_6$]ClO_4·H_2O (**IV-7**)

[NEt_4][Fe(salen)]$_2$[Fe(CN)$_6$]·H_2O (**V-1**)

[Fe(salen)(MeOH)$_2$][Fe(salen)]$_2$[Fe(CN)$_6$]·3H_2O (**V-2**)

[K(18-cr)(2-PrOH)$_2$][Mn(acacen)]$_2$[Fe(CN)$_6$] (**A-1**)

[K(18-cr)(MeOH)$_2$][Mn(5-Clsalen)(H_2O)(MeOH)]$_2$[Fe(CN)$_6$]·4MeOH (**A-2**)

The crystal structures (crystal packing) of the compounds can generally be controlled by the following factors: (i) the coordinative acceptor nature of manganese(III) and iron(III) Schiff base complexes, affected by the salen-type Schiff base ligand (ligand field and steric character); (ii) counter cation which affects greatly the three-dimensional packing of the assembly compounds; (iii) solvent that affects solution structure of the manganese(III) Schiff base complex and hence controls the reaction product.

In Chapter I, various one- and two-dimensional extended compounds obtained by the reaction of [Mn(SB)]$^+$ with [Fe(CN)$_6$]$^{3-}$ (NEt_4^+ and K^+ salts) were described [1-D: **I-1**, **I-2**, 2-D: **I-3a**, **I-3b**, **I-4**, **I-5a**, **I-5b**, **I-6**]. The assembly reaction and crystal structures of the obtained compounds were greatly affected by the factors, (i) and (ii) mentioned above.

In Chapter II, the two-dimensional bimetallic assemblies, K[Mn(3-MeOsalen)]$_2$[M(CN)$_6$] (M = Co^{3+}: **II-1a**, **II-1b**, Mn^{3+}: **II-2**, Cr^{3+}: **II-3**) were studied on their structures and magnetic properties in view of the magnetic interaction between Mn^{3+} and M^{3+} ions. The bulk magnetic behavior of the compounds is affected by the interlayer magnetic interaction and the magnitude of the ordered spins of the two-dimensional network (dipole effect).

In Chapter III, the solvent effect upon the reaction of [Mn(5-Xsalen)]$^+$ (X = Cl and Br) and [Fe(CN)$_6$]$^{3-}$ (NEt_4^+ and K^+ salts) was described [trinuclear: **III-1** (X = Cl, K^+ salt), **III-2** (X = Br, K^+ salt), **III-3** (X = Cl, NEt_4^+ salt), 2-D: **III-4** (X = Cl, NEt_4^+ salt)] (Scheme III.1). The intralayer magnetic interactions of the two 2-D compounds, **I-3b** and **III-4**, were ferromagnetic and ferrimagnetic, respectively, as the result of different Mn-N-C-Fe nature.

In Chapter IV, solvent-capping effect in the assembly reaction of [Mn(SB)]$^+$ with [Fe(CN)$_6$]$^{3-}$ and desolvation reaction from discrete oligomer into extended structure were described [solvent-capped compounds, dinuclear: **IV-1a**, trinuclear: **IV-2a**, **IV-3a**, **IV-4a**, pentanuclear: **IV-5a**, oligomeric mixture: **IV-6a**, **IV-6b**, **IV-7**, desolvated compounds, **IV-1b**, **IV-2b**, **IV-3b**, **IV-4b**, **IV-5b**]. The solvated forms have a discrete oligomeric structure and showed no magnetic ordering. Desolvated compounds, **IV-1b**, **IV-2b**, and **IV-3b**, showed a ferrimagnetic phase transition with spontaneous magnetization, indicating the conversion of the discrete oligomeric core into an extended structure by desolvation reaction.

In Chapter V, the reaction of [Fe(salen)(Cl)] with [Fe(CN)$_6$]$^{3-}$ (NEt_4^+ and K^+ salts) of a the 2-D layered structure were described (**V - 1** and **V - 2**). [Fe(salen)(MeOH)$_2$][Fe(salen)]$_2$[Fe(CN)$_6$]·3H_2O (**V-2**) has a hybrid two-dimensional layered structure consisting of a ferromagnetic layers based on [-Fe(*hs*)-NC-Fe(*ls*)-CN-]$_4$ unit and a paramagnetic layer of [Fe(salen)(MeOH)$_2$]$^+$ as a "spacer". This compound must be important in a viewpoint of the development of the multi-functional materials in future.

In this work three-dimensional compounds like Prussian Blue-type could not be obtained from the reaction between manganese(III) Schiff base complex and hexacyanoferrate(III). This is thought to be due to a steric hindrance occurring between the building blocks, when six molecules of manganese(III) Schiff base complexes are gathered around [Fe(CN)$_6$]$^{3-}$. To produce such three-dimensional compounds, a synthetic approach using a two-dimensional layer and combining the layers with an appropriate spacer bridge is recommended.

As described in this thesis, the reaction of a manganese(III) Schiff base complex and A_3[Fe(CN)$_6$] generally gives the two-dimensional layered compound with the general formula, [A{Mn(SB)}2{Fe(CN)6}]$_\infty$, in which the cation A^+ locates between the layers (see structure of **I-4** and **III-4**). If the cationic part is designed so as to form another layer, a new

type of hybrid two-dimensional layered compounds may be constructed (Scheme 2). Preliminary studies in this line have been made in this thesis and the results are briefly given in Appendix.

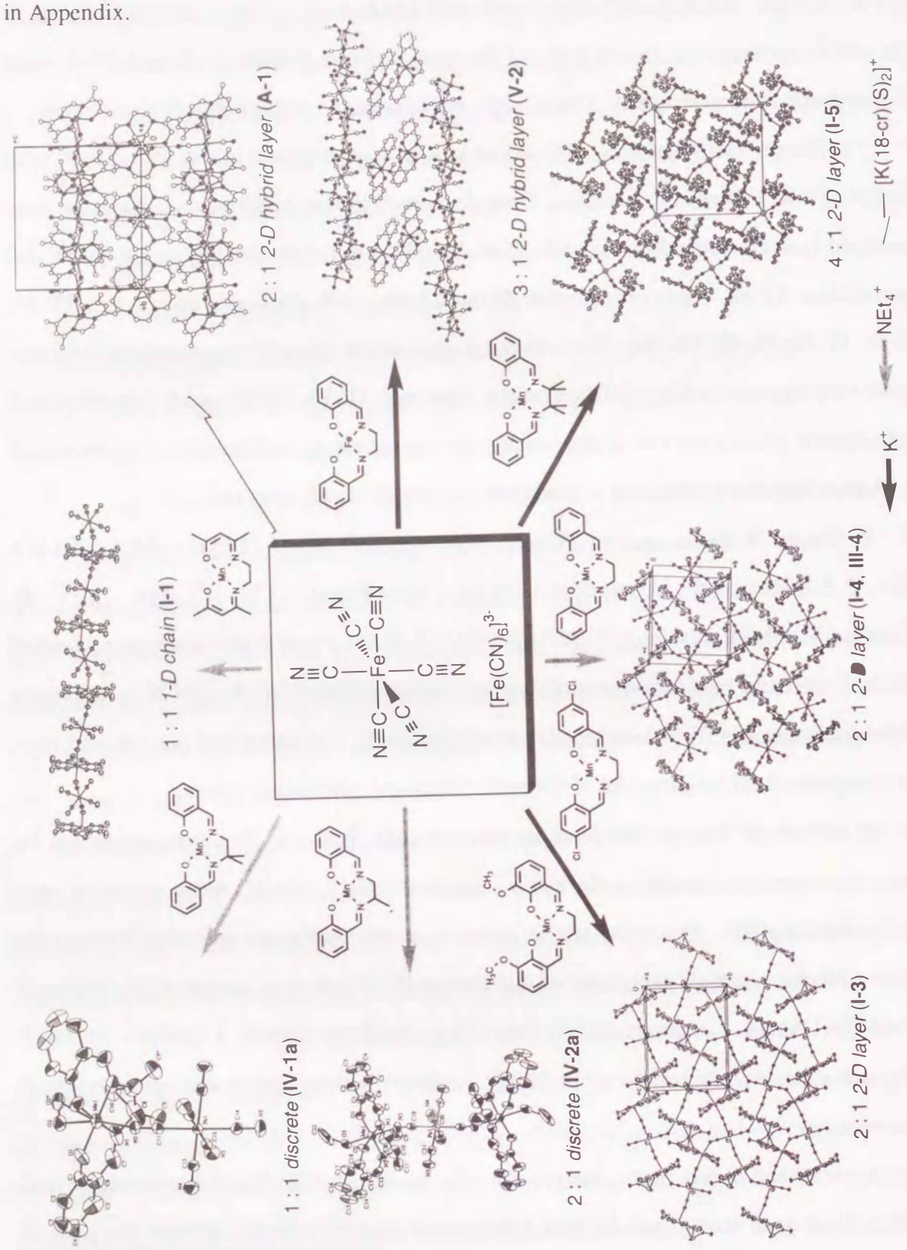

Figure 1. Assembly compounds having the multi-dimensional structure synthesized in this work.

Scheme 1.

Reaction Between Mn(III) Salen-type Complexes and $A_3[Fe(CN)_6]$ ($A = K^+, [NEt_4]^+$)

[Mn(acacen)(Cl)] / *rac*-[Mn(acacmen)(Cl)] —$[NEt_4]_3[Fe(CN)_6]$, in EtOH, 2-PrOH→ 1-D chain compound (1 : 1) **I-1** and **I-2**

$[Mn(3\text{-}MeOsalen)(H_2O)]ClO_4$ —$K_3[M(CN)_6]$, in MeOH, H_2O or DMF/H2O, 2-PrOH→ 2-D layered compound (2 : 1) **I-3a** and **I-3b** **II-1a**, **II-1b**, **II-2**, **II-3**

$[Mn(salen)(H_2O)]ClO_4$
- —$[NEt_4]_3[Fe(CN)_6]$, in MeOH, EtOH→ 2-D layered compound (2 : 1) **I-4**
- —$K_3[Fe(CN)_6]$, in MeOH, H_2O→ Oligomer mixture compound (3 : 1) **IV-6a** and **IV-6b**

$[Mn(saltmen)(H_2O)]ClO_4$
- —$K_3[M(CN)_6]$, in MeOH, H_2O→ 2-D layered compound (4 : 1) **I-5a**, **I-5b** and **I-6**
- —$[NEt_4]_3[Fe(CN)_6]$, in EtOH→ Discrete oligomer compound (4 : 1) **IV-5a**

$[Mn(5\text{-}Xsalen)(H_2O)]ClO_4$ (X = Cl, Br)
- —$K_3[Fe(CN)_6]$, in MeOH, H_2O→ Discrete oligomer compound (2 : 1) **III-1** and **III-2**
- —$[NEt_4]_3[Fe(CN)_6]$, in MeOH→ Discrete oligomer compound (2 : 1) **III-3**
- —$[NEt_4]_3[Fe(CN)_6]$, in DMF/MeCN, 2-PrOH→ 2-D layered compound (2 : 1) **III-4**

$[Mn(saldmen)(H_2O)]ClO_4$ —$[NEt_4]_3[Fe(CN)_6]$, in MeOH, 2-PrOH→ Discrete oligomer compound (1 : 1) **IV-1a**

rac-$[Mn(salmen)(H_2O)]ClO_4$ —$[NEt_4]_3[Fe(CN)_6]$, in MeOH, EtOH→ Discrete oligomer compound (2 : 1) **IV-2a**

rac-$[Mn(salcy)(H_2O)]ClO_4$
- —$K_3[Fe(CN)_6]$, in MeOH, H_2O→ Oligomer mixture compound (4 : 1) **IV-7**
- —$[NEt_4]_3[Fe(CN)_6]$, in MeOH→ Discrete oligomer compound (2 : 1) **IV-3a**

(*R*, *R*)-$[Mn(salcy)(H_2O)]ClO_4$ —$[NEt_4]_3[Fe(CN)_6]$, in MeOH→ Discrete oligomer compound (2 : 1) **IV-4a**

Scheme 2.

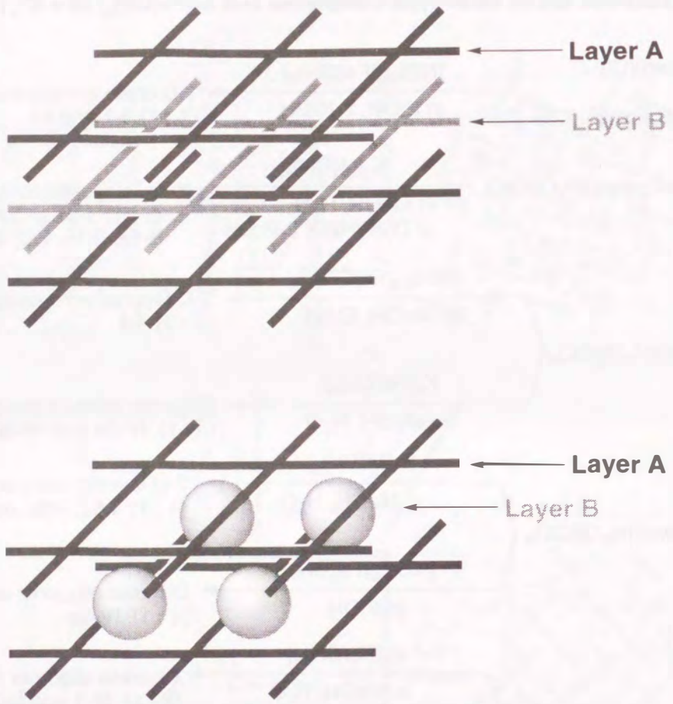

Hybrid two-dimensional layered structure consisting of the foreign layers, A and B.

Appendix

[K(18-cr)(2-PrOH)$_2$][Mn(acacen)]$_2$[Fe(CN)$_6$] (A-1)

Preparation of [K(18-cr)(H$_2$O)$_2$]$_3$[Fe(CN)$_6$]·3H$_2$O. To a suspension of K$_3$[Fe(CN)$_6$] (3.29 g, 10 mmol) in 100 cm^3 of methanol was added a solution of 18-crown-6-ether (7.93 g, 30 mmol) in 150 cm^3 of methanol at room temperature under anaerbic condition and the orenge-yellow suspension was starred for 6 hr at room temperature in a dark. Suspension varied at this point to a yellow solution and this solution was filtered off and concentrated to 30 cm^3 volume by vacume-evaporation apparatus at below 50 °C. From the concentrated solution, the yellow solids were deposited at this point, and finally it was treated by diethylether, washed with diethylether and dried *in vacuo* to obtain the yellow powder samples. Anal. Calcd for $C_{42}H_{90}N_6O_{27}K_3Fe_1$: C, 39.28; H, 7.06; N, 6.54. Found; C, 39.28; H, 7.03; N, 6.59. IR(KBr): $\nu_{C\equiv N}$(cyanide), 2110 cm^{-1}.

Preparation of [K(18-cr)(2-PrOH)$_2$][Mn(acacen)]$_2$[Fe(CN)$_6$] (A-1). To a solution of [Mn(acacen)(Cl)] (155 mg, 0.5 mmol) in 20 cm^3 of ethanol was added a solution of [K(18-cr)(H$_2$O)$_2$]$_3$[Fe(CN)$_6$]·3H$_2$O (642 mg, 0.5 mmol) in 10 cm^3 of ethanol. The resulting solution was filtered, to the filtrate was added 30 cm^3 of 2-propanol, and the dark brown solution was allowed to stand for 2-3 days in a dark room. If this solution was allowed to stand longer than 3 days, the starting materials, [K(18-cr)(H$_2$O)$_2$]$_3$[Fe(CN)$_6$], may deposit as a impurity with Mn-Fe complex. Dark brown crystals were collected by suction filtration, washed with a minimum value of 2-propanol and dried *in vacuo*. These crystals are suitable for the single X-ray crystallographic analysis. Anal. Calcd for $C_{48}H_{76}N_{10}O_{12}K_1Mn_2Fe_1$: C, 48.45; H, 6.44; N, 11.77. Found; C, 48.07; H, 6.34; N, 11.77. IR(KBr): ν[C=N (imine)] 1583 (broad) cm^{-1}; ν[C≡N (cyanide)] 2068 and 2102 cm^{-1}.

Table A.1. Crystallographic Data for [K(18-cr)(2-PrOH)$_2$][Mn(acacen)]$_2$[Fe(CN)$_6$] (**A-1**)

	A-1		
Formula	$C_{42}H_{64}N_{10}O_{12}KMn_2Fe$	α / deg	90
Formula Weight	1105.85	β / deg	105.64(1)
Crystal System	monoclinic	γ / deg	90
Space group	$P2_1/a$ (#14)	V / Å^3	2976.7(9)
T / degC	20	Z	2
λ / Å	0.71069	D_{cal} / gcm^{-3}	1.234
a / Å	13.272(3)	μ(MoKα) / cm^{-1}	7.85
b / Å	15.768(2)	No. of reflections	7401
c / Å	14.771(2)	R[a]	5.6
		Rw[b, c]	5.5

a; $R = \Sigma||F_o|-|F_c||/\Sigma|F_o|$, b; $Rw = [\Sigma w(|F_o|-|F_c|)^2/\Sigma w|F_o|^2]^{1/2}$, c; $w=1/[\sigma^2(Fo)]$.

Table A.2. Fractional Positional Parameters and Isotropic Equivalent Thermal Parameters for Non-Hydrogen Atoms for $[K(18\text{-cr})(2\text{-PrOH})_2][Mn(acacen)]_2[Fe(CN)_6]$ (**A-1**)

atom	x	y	z	B(eq)
Fe	1/2	0	1/2	2.35(1)
Mn	0.17368(4)	0.19034(4)	0.49355(5)	3.88(1)
K	1/2	0	0	4.78(3)
O(1)	0.1415(2)	0.1808(2)	0.6101(2)	4.77(7)
O(2)	0.0599(2)	0.1188(2)	0.4363(2)	4.54(6)
O(3)	0.5256(4)	0.1617(3)	0.0937(4)	9.0(1)
O(4)	0.5862(3)	0.0117(3)	0.1852(2)	7.8(1)
O(5)	0.5954(4)	-0.1436(3)	0.0967(4)	9.1(1)
O(6)	0.3385(3)	-0.0224(4)	0.0861(2)	10.1(1)
N(1)	0.2824(3)	0.2742(3)	0.5415(5)	8.5(1)
N(2)	0.2131(4)	0.2031(4)	0.3750(5)	8.3(2)
N(3)	0.2948(2)	0.0798(2)	0.5226(2)	3.63(7)
N(4)	0.5665(2)	0.1818(2)	0.4615(3)	4.38(8)
N(5)	0.3887(3)	-0.0140(2)	0.2868(2)	4.77(8)
C(1)	0.1152(8)	0.2192(6)	0.7543(5)	13.7(3)
C(2)	0.1673(5)	0.2356(4)	0.6778(4)	7.4(2)
C(3)	0.2342(7)	0.3010(5)	0.6800(6)	11.3(3)
C(4)	0.2886(5)	0.3206(4)	0.617(1)	12.1(3)
C(5)	0.3578(6)	0.3990(4)	0.635(1)	21.0(4)
C(6)	0.340(1)	0.2927(7)	0.473(1)	22.1(7)
C(7)	0.3108(5)	0.2567(9)	0.393(1)	18.2(4)
C(8)	0.218(1)	0.1719(7)	0.2142(7)	21.8(5)
C(9)	0.172(1)	0.1657(7)	0.2974(8)	14.3(5)
C(10)	0.085(1)	0.1161(6)	0.2860(5)	11.9(3)
C(11)	0.0316(5)	0.0944(3)	0.3490(4)	7.0(1)
C(12)	-0.0635(5)	0.0387(4)	0.3267(6)	11.9(2)
C(13)	0.3710(2)	0.0484(2)	0.5161(2)	2.74(6)
C(14)	0.5435(2)	0.1143(2)	0.4759(2)	3.05(7)
C(15)	0.4302(3)	-0.0107(2)	0.3659(2)	3.23(7)
C(16)	0.5239(7)	0.1459(5)	0.1906(7)	10.7(3)
C(17)	0.6071(7)	0.0868(8)	0.2335(5)	11.7(3)
C(18)	0.6415(6)	-0.0603(8)	0.2326(4)	11.6(3)
C(19)	0.5883(6)	-0.1359(7)	0.1892(8)	12.1(3)
C(20)	0.5510(8)	-0.2208(6)	0.051(1)	13.8(4)
C(21)	0.557(1)	-0.2158(6)	-0.047(1)	14.2(4)
C(22)	0.2422(6)	-0.0590(8)	0.0484(5)	12.0(3)
C(23)	0.177(1)	-0.006(2)	0.049(2)	43(1)

Crystal Structure of $[K(18\text{-cr})(2\text{-PrOH})_2][Mn(acacen)]_2[Fe(CN)_6]$ (A-1). A perspective view of the $[Mn_2Fe]$ trimetallic anion, $[\{Mn(acacen)\}_2\{Fe(CN)_6\}]^-$, and potassium 18-crown-6-ether cation, $[K(18\text{-cr})(2\text{-PrOH})_2]^+$, with the numbering scheme of the unique atoms is shown in Figure A.1, and the bond distances and angles are reported in Table A.3. Figure A.2 shows the two-dimensional network structures consisting of a cyclic octamer $[\text{-Mn-NC-Fe-CN-}]_4$ as a net unit which is a view projected along the *c*-axis. Figure A.3 shows the hybrid two-dimensional layer structure, where the figure on left representing two two-dimensional network A and B stacking is a view projected along the *a*-axis and that on right representing stacking is a view projected along the *b*-axis.

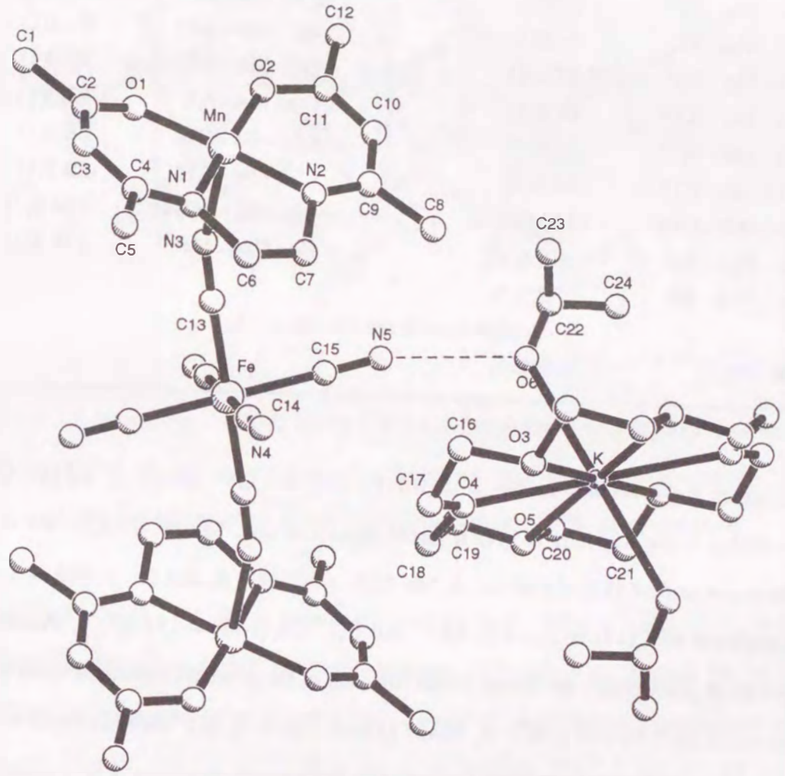

Figure A.1. Perspective view of trinuclear unit $[Mn_2Fe]$ and potassium-crown-ether cation for **A-1** with the atom numbering scheme of the unique atoms.

Table A.3. Relevant Bond Distances (Å) and Angles (deg) for **A-1** with the Estimated Standard Deviations in Parentheses.

		Bond Distances (Å)	
Mn - N1	1.944(4)	Mn - N2	1.968(5)
Mn - N3	2.331(3)	Mn - N4*	2.439(3)
Mn - O1	1.888(3)	Mn - O2	1.892(3)
Fe - C13	1.947(3)	Fe - C14	1.954(3)
Fe - C15	1.955(3)	C13 - N3	1.153(4)
C14 - N4	1.143(4)	C15 - N5	1.151(4)
K - O3	2.877(4)	K - O4	2.672(3)
K - O5	2.792(4)	K - O6	2.794(4)
		Bond Angles (deg)	
N1 - Mn - N3	92.0(1)	N1 - Mn - N4*	81.1(1)
N2 - Mn - N3	84.5(1)	N2 - Mn - N4*	91.4(2)
N3 - Mn - N4*	172.3(1)	O1 - Mn - N3	95.0(1)
O1 - Mn - N4*	88.8(1)	O2 - Mn - N3	93.7(1)
O2 - Mn - N4*	93.0(1)	C13 - Fe - C14	88.5(1)
C13 - Fe - C15	88.0(1)	C14 - Fe - C15	88.7(1)
Mn - N3 - C13	152.0(3)	Mn - N4* - C14*	154.8(3)
Fe - C13 - N3	176.8(3)	Fe - C14 - N4	178.4(3)
Fe - C15 - N5	177.7(3)		
		Hydrogen Bond Distances (Å)	
O6···N5	2.861(5)		

Iron occupies the inversion centers, (1/2,0,1/2), and two CN^- groups of the $[Fe(CN)_6]^{3-}$ moiety bridge to the Mn ions to give a linear trinuclear unit, Mn-NC-Fe-CN-Mn with the bond distances of Fe-C(17) = 1.947(8) Å, Mn-N(3) = 2.286(7) Å, and C(17)-N(3) = 1.126(9) Å and angles of Fe-C(17)-N(3) = 177.9(8) ° and C(17)-N(3)-Mn = 154.4(7) °. Another two CN^- groups of $[Fe(CN)_6]^{3-}$ are bound to the Mn ions of the adjacent trinuclear units with the dimensions of Mn*-N(4)=2.226(7) Å, N(4)-C(18)=1.146(9) Å, Mn*-N(4)-C(18)=146.1(7) °, Fe-C(18)-N(4)=174.4(8) °. Such a Fe-C-N-Mn interaction produces a two-dimensional network, $[Mn_2Fe]_n$, having a repeating cyclic octameric [-Mn-NC-Fe-CN-]$_4$ unit (Figure A.2). The remaining two CN groups do not participate in coordination bridging in the $[Mn_2Fe]_n$ two-dimensional network, but make a hydrogen bond with hydroxy hydrogen of 2-

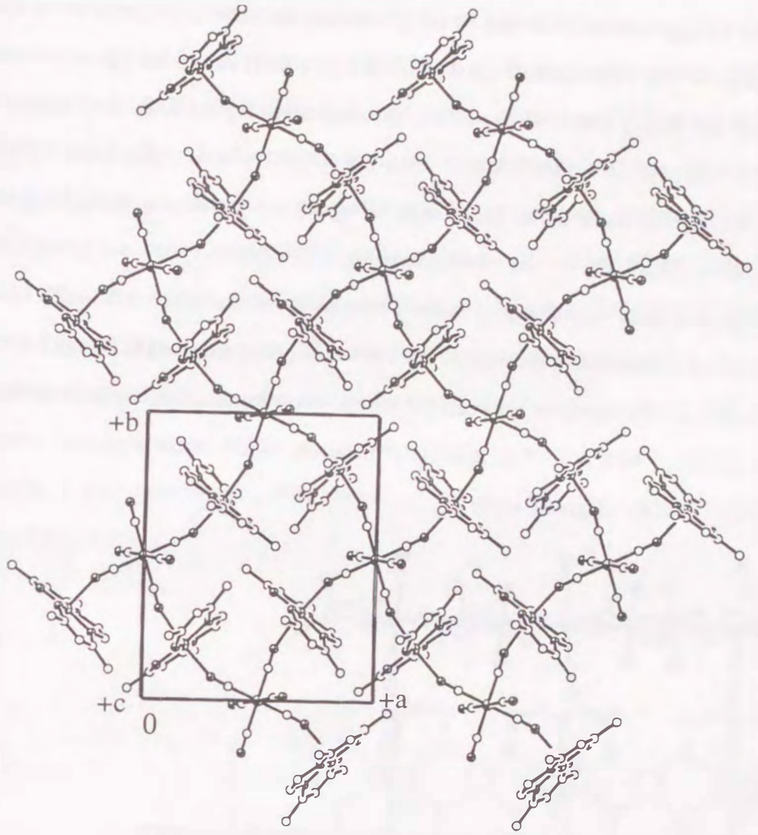

Figure A.2. A projection of **A-1**, along the *c*-axis, showing a two-dimensional network structure in which a net unit is composed of a cyclic octamer structure [-Mn-NC-Fe-CN-]$_4$. This network is similar to that of the isostructural compounds, **II-3b**, **II-4**, and **IV-4**.

propernol in $[K(18\text{-cr})(2\text{-PrOH})_2]^+$ with a distance of N(5)···O(6) = 2.861(5) Å, and as a result, $[Mn_2Fe]_n$ two-dimensional networks connect with each other through $[K(18\text{-cr})(2\text{-PrOH})_2]^+$ by the hydrogen bond (Figure A.3). The Fe-C bonds which participate in the coordination bridging and are involved in the octamer cycle (Fe-C(17)=1.947(8) and Fe-C(18)=1.951(8) Å) are rather shorter in the distance than that participating to the hydrogen bridging mode (Fe-C(19)=1.979(9) Å). Due to the coordination of the CN^- groups, the Mn ion assumes a square bipyramidal six-coordination geometry, in which the two apical sites are

occupied by nitrogen atoms N(3) and N(4)* (* denotes the atom of adjacent unit) with the bond distances of Mn-N(3)=2.286(7) and Mn-N(4)*=2.226(7) Å and the equatorial sites are occupied by the N_2O_2 donor atoms of the quadridentate ligand with the average bond distances of <Mn-N> = 1.985(7)Å and <Mn-O> = 1.903(5) Å. $[K(18\text{-cr})(2\text{-PrOH})_2]^+$ cationic molecule arranges along the a-axis, in which the potassium atom occupies the inversion center (1/2, 0, 0), and the plane consisting of the ether oxygen and potassium atom positions approximately perpendicular to the *a*-axis, as shown in Figure A.3, and it forms the one-dimensional column along the *a*-axis. As a result of positioning of $[K(18\text{-cr})(2\text{-PrOH})_2]^+$ cationic molecule, the distance between $[Mn_2Fe]_n$ two-dimensional layers is widely (the interlayer distance: 14.8 Å). This interlayer distance affects to the magnetic interaction between layers (see the magnetic study).

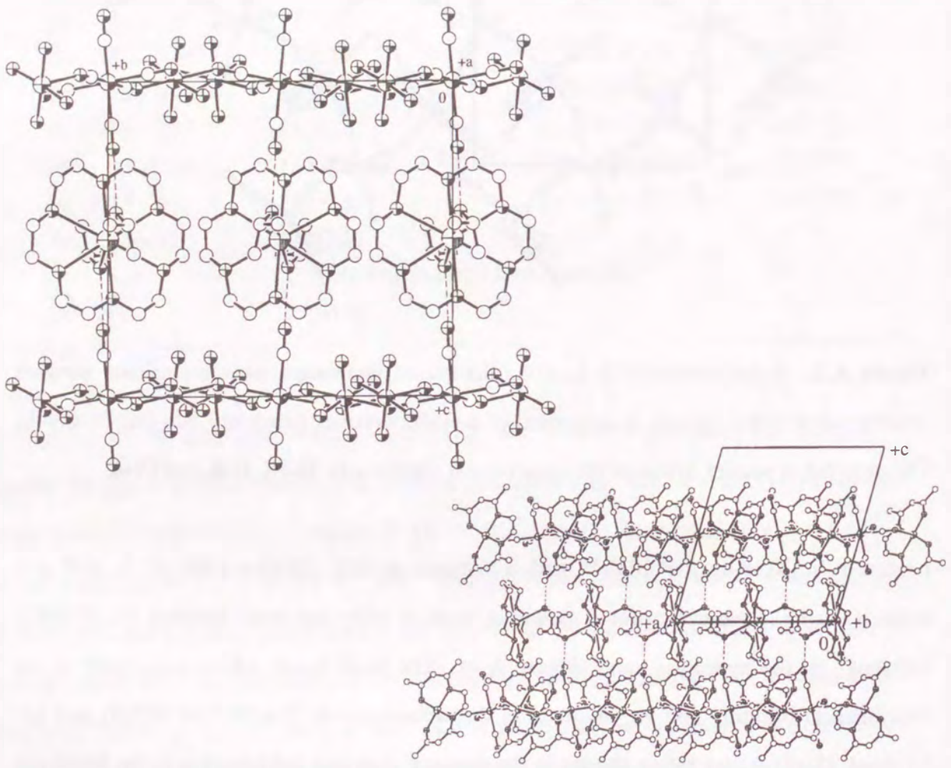

Figure A.3. Projections of **A-1** along two axis perpendicular to the two-dimensional network sheet, (top) along the *a*-axis, (bottom) along the *b*-axis.

The compound is isostructural to metamagnet $K[Mn(3\text{-MeOsalen})]_2[Fe(CN)_6]\cdot 2DMF$ (**I-3b**), ferrimagnet $[NEt_4][Mn(salen)]_2[Fe(CN)_6]$ (**I-4**), and metamagnet $[NEt_4][Mn(5\text{-Clsalen})]_2[Fe(CN)_6]$ (**III-4**) described above Chapter, except for a difference of the counter cation. However, as the counter cation for this compound is the largest to that for the above mentioned compounds, the interlayer distance is the most widely (compound **A-1**: 14.8 Å, $K[Mn(3\text{-MeOsalen})]_2[Fe(CN)_6]\cdot 2DMF$ (**I-3b**): 13.1 Å, $[NEt_4][Mn(salen)]_2[Fe(CN)_6]$ (**I-4**): 13.0 Å, $[NEt_4][Mn(5\text{-Clsalen})]_2[Fe(CN)_6]$ (**III-4**): 13.7 Å), and $[K(18\text{-cr})(2\text{-PrOH})_2]^+$ is no longer as a counter cation, it oneself forms a cationic two-dimensional layer (consisting of the one-dimensional column along the *a*-axis) between $[Mn_2Fe]$ anionic layers (Figure A.3 and Scheme A.1). As a result, this compound is a hybrid two-dimensional layered compound consisting of an anionic layer, $[\{Mn(acacen)\}_2\{Fe(CN)_6\}]_n^{n-}$, and a cationic layer, $[K(18\text{-cr})(2\text{-PrOH})_2]_n^{n+}$.

Scheme A.1.

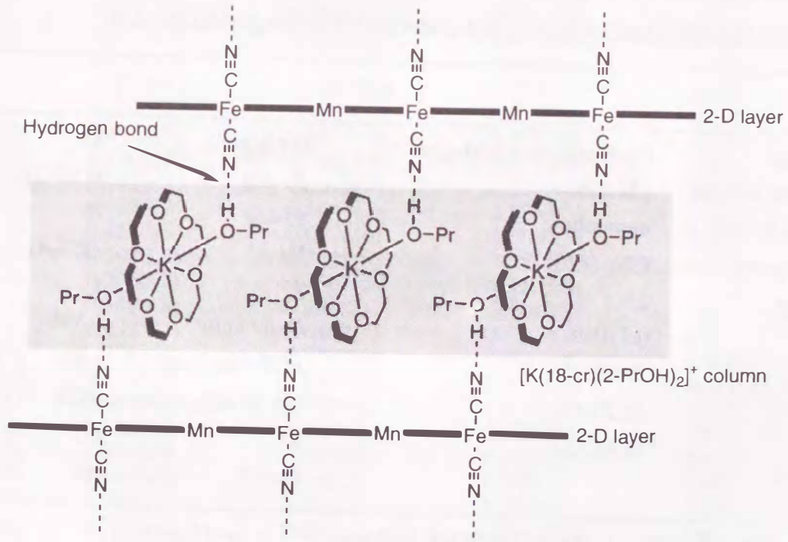

[K(18-cr)(MeOH)$_2$][Mn(5-Clsalen)(H$_2$O)(MeOH)]$_2$[Fe(CN)$_6$]·4MeOH (A-2)

Preparation of [K(18-cr)(MeOH)$_2$][Mn(5-Clsalen)(H$_2$O)(MeOH)]$_2$[Fe(CN)$_6$]·4MeOH (A-2). To a solution of [Mn(5-Clsalen)(H$_2$O)]ClO$_4$ (254 mg, 0.5 mmol) in 30 cm^3 of methanol was added a solution of [K(18-cr)(H$_2$O)$_2$]$_3$[Fe(CN)$_6$]·3H$_2$O (642 mg, 0.5 mmol) in 20 cm^3 of methanol. The resulting solution was filtered without a starring and the dark brown solution was allowed to stand for 2 days in a dark room. Dark brown needle shape crystals were obtained. The crystals easily efflorescence in the air. These were collected by suction filtration, washed with a minimum value of ethanol and dried in air to obtain the powder sample. Anal. Calcd for desolvated powder sample of **A-2**, $C_{48}H_{76}N_{10}O_{12}K_1Mn_2Fe_1$: C, 48.45; H, 6.44; N, 11.77. Found: C, 48.07; H, 6.34; N, 11.77. IR(KBr): ν[C=N (imine)] 1583 (broad) cm^{-1}; ν[C≡N (cyanide)] 2068 and 2102 cm^{-1}.

Table A.4. Crystallographic Data for [K(18-cr)(MeOH)$_2$][Mn(5-Clsalen)(H$_2$O)(MeOH)]$_2$[Fe(CN)$_6$]·4MeOH (**A-2**)

	A-2		
Formula	$C_{58}H_{84}N_{10}O_{20}KMn_2Fe$	α / deg	90
Formula Weight	1587.99	β / deg	98.83(2)
Crystal System	monoclinic	γ / deg	90
Space group	*C*2/*c* (#15)	V / Å^3	7553(4)
T / degC	23	Z	4
λ / Å	0.71069	D_{cal} / gcm^{-3}	1.396
a / Å	29.065(5)	μ(MoKα) / cm^{-1}	7.86
b / Å	14.261(8)	No. of reflections	9228
c / Å	18.443(6)	R[a]	6.2
		Rw[b, c]	6.7

a; $R = \Sigma||F_o|-|F_c||/\Sigma|F_o|$, b; $Rw = [\Sigma w(|F_o|-|F_c|)^2/\Sigma w|F_o|^2]^{1/2}$, c; $w=1/[\sigma^2(Fo)]$.

Table A.5. Relevant Bond Distances (Å) and Angles (deg) for **A-2** with the Estimated Standard Deviations in Parentheses.

atom	x	y	z	B(eq)
Fe(1)	1/4	3/4	1/2	3.39(3)
Mn(1)	0.26601(4)	0.30954(8)	0.37775(6)	3.60(2)
K(1)	1/2	0.0609(2)	1/4	8.2(1)
Cl(1)	0.0807(1)	0.0106(2)	0.2056(2)	10.3(1)
Cl(2)	0.4718(1)	0.5146(2)	0.5871(2)	9.4(1)
O(1)	0.3101(2)	0.2903(3)	0.4624(2)	4.0(1)
O(2)	0.2428(2)	0.1871(3)	0.3785(2)	4.3(1)
O(3)	0.2113(2)	0.3561(3)	0.4446(2)	4.0(1)
O(4)	0.3198(2)	0.2675(4)	0.3089(3)	5.6(2)
O(5)	0.4559(5)	0.056(2)	0.3730(8)	22.9(7)
O(6)	0.5634(7)	-0.122(2)	0.3001(9)	23.4(9)
O(7)	0.5968(6)	0.043(2)	0.347(1)	27(1)
O(8)	0.541(1)	0.267(1)	0.294(1)	25(1)
O(9)	0.0747(4)	0.2920(8)	0.0835(6)	13.3(4)
O(10)	0.1172(7)	0.456(1)	0.122(1)	24.5(9)
N(1)	0.2845(2)	0.4420(4)	0.3703(3)	3.8(1)
N(2)	0.2238(2)	0.3407(4)	0.2855(3)	4.0(1)
N(3)	0.2297(3)	0.5385(5)	0.4918(4)	5.7(2)
N(4)	0.2923(3)	0.7341(6)	0.6631(4)	7.1(2)
N(5)	0.3460(3)	0.7202(6)	0.4518(5)	7.2(3)
C(1)	0.3464(3)	0.3442(5)	0.4874(4)	3.9(2)
C(2)	0.3806(3)	0.3072(6)	0.5426(4)	5.2(2)
C(3)	0.4184(3)	0.3595(7)	0.5728(5)	6.1(2)
C(4)	0.4235(3)	0.4494(7)	0.5491(5)	6.0(2)
C(5)	0.3912(3)	0.4882(6)	0.4954(5)	5.3(2)
C(6)	0.3522(3)	0.4361(5)	0.4645(4)	4.1(2)
C(7)	0.3191(3)	0.4818(5)	0.4082(4)	4.3(2)
C(8)	0.2519(3)	0.4972(5)	0.3174(4)	4.6(2)
C(9)	0.2345(3)	0.4313(6)	0.2537(4)	5.1(2)
C(10)	0.1921(3)	0.2873(5)	0.2521(4)	4.0(2)
C(11)	0.1802(2)	0.1963(5)	0.2764(4)	3.8(2)
C(12)	0.1421(3)	0.1513(6)	0.2369(4)	4.9(2)
C(13)	0.1289(3)	0.0647(7)	0.2563(5)	5.6(2)
C(14)	0.1543(3)	0.0176(6)	0.3149(5)	5.4(2)
C(15)	0.1920(3)	0.0598(5)	0.3551(4)	4.3(2)
C(16)	0.2060(2)	0.1507(5)	0.3378(4)	3.7(2)
C(17)	0.3496(8)	0.196(2)	0.3262(9)	24(1)
C(18)	0.2375(3)	0.6169(5)	0.4952(4)	4.2(2)
C(19)	0.2761(3)	0.7392(6)	0.6023(4)	4.4(2)
C(20)	0.3105(3)	0.7302(5)	0.4707(4)	4.7(2)
C(21)	0.469(1)	0.109(3)	0.434(1)	38(2)
C(22)	0.5212(6)	-0.153(2)	0.273(1)	16(1)
C(23)	0.6038(9)	-0.061(3)	0.339(2)	24(1)
C(24)	0.5926(6)	0.142(3)	0.346(1)	17(1)
C(25)	0.568(1)	0.208(1)	0.332(2)	16(1)
C(26)	1/2	0.311(3)	1/4	18(2)
C(27)	0.0355(5)	0.237(1)	0.057(1)	13.4(6)
C(28)	0.1491(8)	0.496(2)	0.081(1)	25(1)

Crystal Structure of [K(18-cr)(MeOH)$_2$][Mn(5-Clsalen)(H$_2$O)(MeOH)]$_2$[Fe(CN)$_6$]·4MeOH (A-2). An ORTEP drawing of hydrogen bonded monomer mixture [Mn(5-Clsalen)(H$_2$O)(MeOH)]$_2$[Fe(CN)$_6$]$^-$ and the hydrogen bonding mode with the numbering scheme of the unique atoms is shown in Figure A.4, and the bond distances and angles are reported in Table A.6.

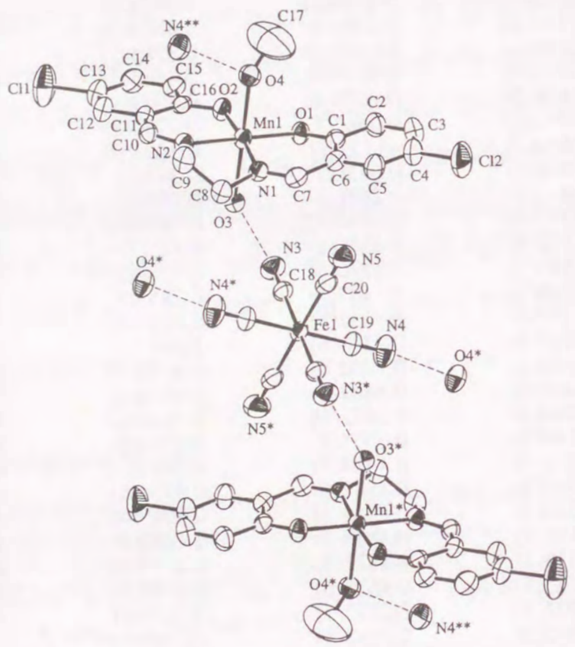

Figure A.4. ORTEP drawing of hydrogen bonded monomer mixture [Mn(5-Clsalen)(H$_2$O)(MeOH)]$_2$[Fe(CN)$_6$]$^-$ for **A-2** with the atom numbering scheme of the unique atoms.

The reaction between [Mn(5-Clsalen)(H$_2$O)]ClO$_4$ and [K(18-cr)(H$_2$O)$_2$]$_3$[Fe(CN)$_6$]·3H$_2$O in methanol solution gave a hydrogen bonded monomer mixture. The construction of this compound must be greatly affected with the effect of the crystal packing by counter cation [K(18-cr)(MeOH)$_2$]$^+$. Because as described in Chapter III, the assembly reaction using [NEt$_4$]$_3$[Fe(CN)$_6$] instead of [K(18-cr)(H$_2$O)$_2$]$_3$[Fe(CN)$_6$]·3H$_2$O has given the coordination two-dimensional network structure consisting of the octamer net [-Mn-NC-Fe-CN-]$_4$. Manganese(III) ion assumes a square bipyramidal six-coordination

geometry, in which the two apical sites are occupied by oxygen atoms O(3) and O(4) originated H$_2$O and MeOH molecules, respectively, with the bond distances of Mn-O(3) = 2.255(5) and Mn-O(4) = 2.242(6) Å and the equatorial sites are occupied by the N$_2$O$_2$ donor atoms of the quadridentate 5-Clsalen^{2-} ligand with the average bond distances of <Mn-N> = 1.983 Å and <Mn-O> = 1.878 Å. [Fe(CN)$_6$]$^{3-}$ moiety is merely medium of the hydrogen bond between nitrogen atoms and the hydrogen of H$_2$O and MeOH of Mn(III) moiety, with bond distances of O3···N4 = 2.768(8) and O4···N3 = 2.685(8) Å. Figure A.5. a) shows the hydrogen bonded two-dimensional network consisting of hydrogen bonded octanuclear net [···(MeOH)Mn(H$_2$O)···NC-Fe-CN···]$_4$. [K(18-cr)(MeOH)$_2$]$^+$ as a counter cation locates in the two-dimensional layers as shown in Figure A.5. b). Since crown-ether moiety of [K(18-cr)(MeOH)$_2$]$^+$ has complicated disordering, the atomic coordinates for crown-ether moiety were not able to be determined completely.

Table A.6. Relevant Bond Distances (Å) and Angles (deg) for **A-2** with the Estimated Standard Deviations in Parentheses.

	Bond Distances (Å)		
Mn - N1	1.974(6)	Mn - N2	1.989(6)
Mn - O1	1.883(4)	Mn - O2	1.873(5)
Mn - O3	2.256(5)	Mn - O4	2.241(6)
Fe - C18	1.931(8)	Fe - C19	1.928(7)
Fe - C20	1.939(10)	C18 - N3	1.142(9)
C19 - N4	1.150(9)	C20 - N5	1.15(1)
	Bond Angles (deg)		
N1 - Mn - O3	88.7(2)	N1 - Mn - O4	89.8(2)
N2 - Mn - O3	90.5(2)	N2 - Mn - O4	88.1(2)
O3 - Mn - O4	178.1(2)	O1 - Mn - O3	92.1(2)
O1 - Mn - O4	89.2(2)	O2 - Mn - O3	89.2(2)
O2 - Mn - O4	92.2(2)	C18 - Fe - C19	90.5(3)
C18 - Fe - C20	90.9(3)	C19 - Fe - C20	91.4(3)
Fe - C18 - N3	179.3(7)	Fe - C19 - N4	178.6(8)
Fe - C20 - N5	178.1(8)		
	Hydrogen Bond Distances (Å)		
O3···N3	2.768(8)	O4···N4*	2.684(8)

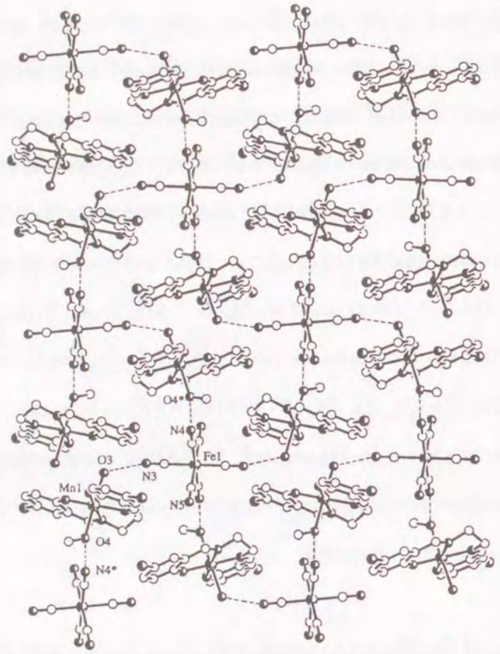

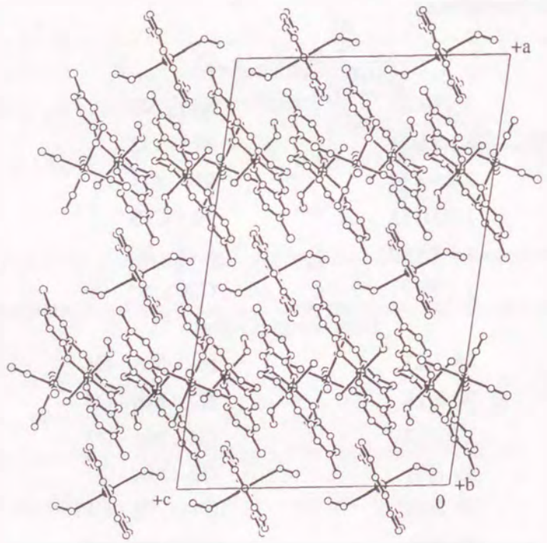

Figure A.5. a) Hydrogen bonded two-dimensional network structure, in which a net unit is composed of a hydrogen bonded cyclic $[\cdots(MeOH)Mn(H_2O)\cdots NC\text{-}Fe\text{-}CN\cdots]_4$. b) Perpendicular view against the projection of 2-D network, $[K(18\text{-cr})(MeOH)_2]^+$ as a counter cation locates in the interlayers with arrangement of one-dimensional column.

Acknowledgment

The present work has been carried out under the supervision of Professor Hisashi Okawa and Professor Naohide Matsumoto at Department of Chemistry, Faculty of Science, Kyushu University. The author is very grateful to them for their advises and valuable discussions throughout this study.

The all works resulted from the collaboration with Professor Carlo Floriani, Institut de Chimie Minéral et Analytique, Université de Lausanne, and Dr. Nazzareno Re, Dipartimento di Chimica, Universitá di Perugia. The author would like to express gratitude to them for their advises and valuable discussions, especially, in the magnetic studies of this study. The author would like to be grateful to Dr. Emma Gallo and Dr. Raffaella Crescenzi, Institut de Chimie Minéral et Analytique, Université de Lausanne for the magnetic measurement.

He deeply thanks Dr. Masaaki Ohba for useful discussion, and Mr. Hidenori Ieda for his help as co-worker (Chapter IV). He also thanks all the members of the Coordination Chemistry Laboratory of Kyushu University for their kind encouragement during this work.

At the last, the author is grateful to Professor Yonezo Maeda and Assoc. Professor Kazuhiro Takahashi for reviewing this thesis and valuable discussion.